Integrating Electrochemical Sensing with Droplet Microfluidics for Metabolic Engineering

Nicholas F.O. Crudele

A Thesis

in

The Department

of

Biology

Presented in Partial Fulfillment of the Requirements

For the Degree of Master of Science (Biology) at

Concordia University

Montreal, Québec, Canada

April 2024

© Nicholas Crudele, 2024

CONCORDIA UNIVERSITY

SCHOOL OF GRADUATE STUDIES

This is to certify that the thesis is prepared

By: Nicholas Francesco O'Hara Crudele

Entitled: Integrating Electrochemical Sensing with Droplet Microfluidics for Metabolic Engineering

and submitted in partial fulfilment of the requirements for the degree of

Master of Science (Biology)

complies with the regulations of the University and meets the accepted standards with respect to originality and quality.

Signed by the final examining committee:

_____ Chair
Dr. Vincent Martin

_____ External Examiner
Dr. David Kwan

_____ Examiner
Dr. Brandon Helfield

_____ Thesis Supervisor
Dr. Steve Shih

Approved by

_____
Dr. Robert Weladji, Graduate Program Director

May 1, 2024

_____
Dr. Pascale Sicotte. Dean of Faculty of Arts & Science

Abstract

Integrating Electrochemical Sensing with Droplet Microfluidics for Metabolic Engineering

Nicholas Crudele

Measuring metabolites produced by large libraries of metabolically engineered yeast requires high throughput screening technology. Current screening methods use mass spectrometry to measure metabolites. Higher throughput detection methods are available, however they rely on fluorescent detection. Measuring non-fluorescent metabolites requires an alternative detection method integrated in the screening system. Herein, we introduce an electrochemical sensor, that can be integrated with droplet microfluidics to detect a key branch point molecule in opiate biosynthesis: (*S*)-reticuline, which is produced by metabolically engineered yeast. This platform technology could be used to screen a heterogenous library consisting of engineered yeast that secrete (*S*)-reticuline. Demonstrating that yeast cells in a population, which produce high titers of (*S*)-reticuline can be detected using this screening system will open the door to screening libraries of micro-organisms that produce other electroactive, non-fluorescent secreted metabolites.

Acknowledgements

I would like to express my sincere appreciation to those that have supported me throughout the research and writing process of this thesis.

I would like to thank Dr. Steve Shih for taking me on as a Master's student, for his ongoing support and encouragement; especially during the experimental process, and foremost for the freedom he gave me to explore science and engineering through the lens of this project in the directions I found interesting.

Next, I would like to thank all my friends and research colleagues in our lab for creating a welcoming environment. Their willingness and eagerness to guide, brainstorm, and troubleshoot problems played a huge role in getting comfortable in the lab and made understanding complex ideas more straightforward. Working with these colleagues was a great pleasure for me and I learned a lot. A special thanks to Dr. Laszlo Kekedy-Nagy, Jay Pimprikar and Aniket Kandalkar for their broad involvement in many aspects of this research project.
I would also like to thank Dr. Darius Rackus for his insightful advice, and his student Kathy Li for sharing her protocols and data relating to carbon paste electrode fabrication.

I would like to thank Dr. Marek Majewski and his student Joseph-Daniel Chiong for the SEM imaging of carbon paste electrode sensors. I am also grateful to the members of my committee, Dr. Vincent Martin and Dr. Brandon Helfield, for their valuable feedback and suggestions. I would like to thank the Natural Sciences and Engineering Research Council for the NSERC-CREATE SynBioApps program fellowship acceptance, and Lallemand Inc. and the Center for Applied Synthetic Biology for the Lallemand Bioprocessing Scholarship.

Finally, I would like to thank all my family and friends. My biggest and sincerest appreciation to my father, brother and sister for believing in me and inspiring me to follow my dreams. Your unconditional love and unwavering support in my decisions and in anything I undertake have been my biggest source of strength. To the rest of my family and friends, thank you for all the memories and support throughout this journey. This work would not have been possible without the help and support of all of these people. I am truly grateful to each one of them.

Contribution of Authors

Nicholas F.O. Crudele, László Kékedy-Nagy, Jay Pimprikar, Aniket Kandalkar, and Steve C.C. Shih designed the experiments. Nicholas F.O. Crudele, Jay Pimprikar, and Aniket Kandalkar fabricated the devices. Nicholas F.O. Crudele conceptualized and designed the sensor, Nicholas F.O. Crudele, Jay Pimprikar, and Aniket Kandalkar engineered the sensor. Nicholas F.O. Crudele, Jay Pimprikar, and Aniket Kandalkar performed electrochemical measurements.

Measurements for **Figure 3-1** were performed by Nicholas F.O. Crudele and Aniket Kandalkar. The devices in **Figure 3-2a** were designed and fabricated by Nicholas F.O. Crudele. The sensor in **Figure 3-2c** was designed by Nicholas F.O. Crudele, the fabrication process for Cr-CPE was outlined by Nicholas F.O. Crudele, the chromium wire geometry was designed by Jay Pimprikar. SEM sample preparation for **Figure 3-2b,d** was done by Aniket Kandalkar and Nicholas F.O. Crudele and the SEM analysis was performed by Joseph-Daniel Chong in the laboratory of Dr. Majewski. The electrochemical measurement in **Figure 3-3a** was performed by Aniket Kandalkar. The electrochemical measurement in **Figure 3-3b,c** was performed by Nicholas F.O. Crudele and Aniket Kandalkar. The experiment in **Figure 3-3d,e** was adapted from a previous experiment performed by Nicholas F.O. Crudele, while the electrochemical measurement was performed by Jay Pimprikar. The experimental design and electrochemical measurements in **Figure 3-4** were performed by Nicholas F.O. Crudele and Jay Pimprikar, the LC/MS sample preparation was performed by Jay Pimprikar, and Aniket Kandalkar, the LC/MS analysis was performed by Dr. Heng Jiang. The diagram in **Figure 3-5a** was created by Nicholas F.O. Crudele. The experiment in **Figure 3-5b,c** was performed by Nicholas F.O. Crudele and Aniket Kandalkar.

The experiment in **Figure 3-5d,e** was performed by Nicholas F.O. Crudele and Jay Pimprikar. Nicholas F.O. Crudele analyzed all data, performed all graphical and statistical analysis. James M. Perry contributed early experimental design ideas. Chiara L. Alves created engineering diagrams of the device. All authors reviewed the final thesis and approved of the contents.

Table of Contents

List of Figures

List of Tables

List of Calculations

List of Equations

List of Abbreviations

1.	**LC/MS**	liquid chromatography coupled mass spectrometry
2.	**THIQ**	tetrahydroisoquinoline
3.	**BIA**	benzoisoquinoline alkaloid
4.	***P. somniferum***	*Papaver somniferum*
5.	***E. coli***	*Escherichia coli*
6.	***S. cerevisiae***	*Saccharomyces cerevisiae*
7.	**L-DOPA**	L-3,4-dihydroxyphenylalanine
8.	**DODC**	Dopa Decarboxylase
9.	**NCS**	Norcauclaurine Synthase
10.	**UV**	Ultraviolet
11.	**CRAPS**	Chromosomal Repair Assisted Pathway Shuffling
12.	**PDMS**	Polydimethylsiloxane
13.	**FACS**	fluorescence activated cell sorting
14.	**FADS**	fluorescence activated droplet sorting
15.	**CE**	counter electrode
16.	**WE**	working electrode
17.	**RE**	reference electrode
18.	**Red**	reduced form of analyte
19.	**Ox**	oxidized form of analyte
20.	**CV**	cyclic voltammetry
21.	**DPV**	differential pulse voltammetry

22. **CA** chronoamperometry
23. **$I_{p,a}$** oxidation peak current
24. **$I_{p,c}$** reduction peak current
25. **$E_{p,a}$** oxidation peak potential
26. **$E_{p,c}$** reduction peak current
27. **E_{init}** initial potential
28. **E_{app}** applied potential
29. **4-AP** 4-aminophenol
30. **PBS** phosphate buffered saline
31. **IPA** isopropyl alcohol
32. **IPA** Isopropyl Alcohol
33. **DI** deionized
34. **Si** silicon
35. **Min** minute
36. **S** second
37. **w/w** weight/weight
38. **OD** outside diameter
39. **Cr-CPE** chromium carbon paste electrodes
40. **APTES** (3-Aminopropyl)triethoxysilane
41. **GC** Glassy carbon
42. **CP-PDMS** carbon paste-PDMS electrodes
43. **YPD** yeast peptone dextrose
44. **SCS** synthetic complete

45. **YNB** yeast nitrogen base

46. **ANOVA** analysis of variance

47. **OD_{600}** optical density at 600nm wavelength

48. **HFE** hydrofluoroether

Chapter 1 Introduction

In this section, I will introduce metabolic engineering and the importance of (S)-reticuline. I will provide rationale for improving the yield of (S)-reticuline using metabolic engineering and provide a brief literature review of studies that use metabolic engineering to produce (S)-reticuline. Next, I will describe the need for high throughput analysis systems to further improve the yield of (S)-reticuline. Then I will describe existing high throughput screening technology using droplet microfluidics. Following this, I will demonstrate the need for integrating electrochemical sensors with droplet microfluidics. After which I will introduce electrochemistry and its use as an analytical technique, as well as how it has been integrated with microfluidics. Finally, I will outline the objectives of the thesis.

1.1 Metabolic engineering

1.1.1 Approaches to strain improvement

An early example of harnessing the metabolism of micro-organisms is the production of alcohol by yeast fermentation, which dates back to the neolithic period[1]. Taking advantage of this metabolic process allowed humans to use yeast cells as factories to produce a valuable compound. Various approaches to manipulate the metabolism of micro-organisms to improve their utility have been implemented since. These include classical strain improvement[2], genome shuffling[3], and metabolic engineering[4]. In classical strain improvement, a heterogeneous population of cells is subject to successive rounds of selective pressure. This approach has led to improved strains of micro-organisms, including yeast isolates with accelerated sugar utilization[2]. Classical strain

improvement is slow and leads to the accumulation of unintended mutations which are difficult to lose. Genome shuffling uses sexual reproduction to improve the genetic diversity of populations that are subjected to selective pressure. Genome shuffling has been used to create comparable titers of an antibiotic (tylosin) in fewer rounds of mutation and selection than classical strain improvement[3]. Classical strain improvement and genome shuffling are effective in cases where a selective pressure can be used to screen for mutants with the desired phenotype, such as antibiotic resistance[3], or sugar utilization[2]. Metabolic engineering is a strain improvement approach which uses precision genome engineering tools to introduce new metabolic pathways into organisms[5]. These new metabolic pathways produce metabolites that are not produced by wild type organisms[6], including food ingredients[7,8], industrial chemicals[9,10] and pharmaceutical compounds[11].

1.1.2 Metabolic engineering workflow

The workflow that is used to engineer these organisms for metabolite production follows the engineering cycle (**Figure 1-1**). First, a biosynthesis pathway is selected. A biosynthesis pathway is composed of enzymes that catalyze a series of reactions, leading to the desired product. These enzymes must be elucidated in the native host organism, often a plant[12,13]. A host micro-organism is selected to express the pathway of interest. The most important selection criterion is the host organism's native metabolic pathways[14]. The most common organisms used for metabolic engineering are domesticated laboratory species of bacteria and yeast[15]. Bacteria have been engineered for biosynthesis of the grape flavour compound methyl anthranilate[8], acetone, isopropanol[9] and human insulin[11]. For other applications, it is more convenient to start with a metabolite that is part of a yeast metabolic pathway, such as the yeast Ehrlich, mevalonate, and

shikimate pathways which naturally produce fusel alcohols[16], sterols[17] and amino acids[18]. Modifying these yeast metabolic pathways allows the production of pharmaceuticals including opioids[19] and compounds used in the chemical industry[18,20]. Yeast is also used as a host organism in circumstances which require the expression of membrane-localized plant enzymes, since yeast has an endomembrane system that allows the functional expression of these enzymes[21]. Using yeast to express membrane-localized plants enzymes has created an alternative method to produce some plant derived pharmaceuticals, that are otherwise produced using extraction from rare plants[22], or by chemical synthesis[23]. After host and pathway selection, cloning tools such as yeast in vivo DNA assembly are used to assemble the DNA parts, and CRISPR-Cas9 is used to deliver the genes into the genome of the host micro-organism[22]. New combinatorial techniques allow the assembly of biosynthesis pathways using multiple homologs of each gene in the pathway[24]. After the build phase, the test phase uses analytical techniques including Liquid Chromatography coupled Mass Spectrometry (LC/MS)[23], fluorescence detection[25] and high throughput automation[26] to quantify metabolites in the engineered pathway. The results are used to inform new design decisions, to improve yield, or produce new metabolites.

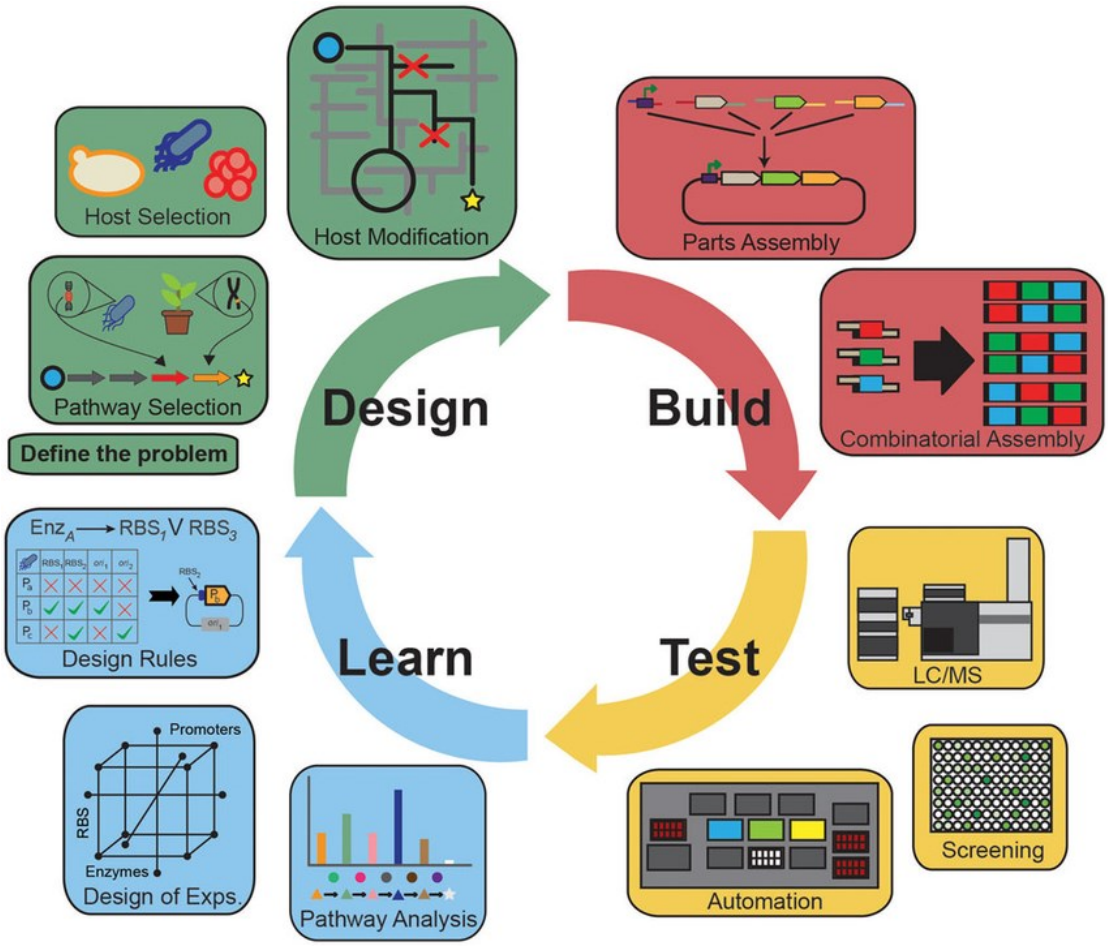

Figure 1-1. The metabolic engineering cycle using synthetic biology approaches

In the design phase, a host micro-organism for expression of the heterologous pathway is selected, as well as a biosynthesis pathway. A strategy is outlined as to which genes need to be expressed in that host organism, and which biosynthesis pathways in the host organism need to be downregulated or knocked down. In the build phase, DNA parts are assembled using cloning techniques. Multiple homologs of each part can be assembled using combinatorial assembly and delivered to the host micro-organism. To validate that the heterologous biosynthesis pathway is working, i.e. the micro-organism is producing the product of interest, analytical tools including LC/MS, and fluorescence detection are used. Recent studies have used high throughput automation equipment for testing large numbers of samples very quickly. The data from the test step is used to learn about bottlenecks in the biosynthesis pathway, for design of experiments, and to identify design rules for future experiments. Reproduced with permission from Frontiers[27].

1.1.3 Rationale for improving opiate production with metabolic engineering

Producing drugs using metabolically engineered micro-organisms solves two problems: low yield (product per feedstock reactant), and declining innovation in pharmaceutical development. The

current industrial standard (chemical synthesis) methods used for producing 3 kg of morphine require a hectare of poppies[28]. This is currently the only method to produce sufficient mass (titer) of morphine for industrial use. The second problem is known as Eroom's Law: a declining trend in innovation and increasing costs in drug development over time[29]. For example, there are 30% fewer therapeutics approved for cardiovascular disease between 2000-2009 compared to the previous decade[29]. Low yield and Eroom's Law demonstrate the need for alternative pharmaceutical development methods.

Metabolic engineering aims to manipulate the metabolism of micro-organisms to improve the yield of pharmaceutical compounds and to deliver new to nature compounds that are structurally like existing drugs. Drugs produced using metabolic engineering include the chemotherapy drug vinblastine[22], cannabinoids[30], tryptamines[31] the malaria treatment artemisinin[32], and insulin[33] for diabetes treatment. Drug production using metabolically engineered microbes isn't just happening in academic research laboratories; half of the world's insulin is produced using recombinant yeast[34], metabolic engineering for the production of artemisinin has been approved by the WHO, and is produced at industrial titers[32]. The production of these drugs at industrial scale using metabolic engineering points towards a future where metabolic engineered micro-organisms are used for the production of other drugs. The most exciting recent work in metabolic engineering for drug production is the production of compounds in the tetrahydroisoquinoline (THIQ) class[35] which are used in a broad range of pharmaceutical applications.

1.1.4 Model system: (*S*)-reticuline in opioid production

THIQ alkaloids include drugs used for treatment of Parkinson's disease[36] and Huntington's disease[37]. The benzoisoquinoline alkaloid (BIA) class of THIQ's include the opiate drugs morphine and codeine, which are on the WHO list of essential medicines[38], and are derived from (*S*)-reticuline (**Figure 1-2**). Since THIQ's are naturally produced in low yields by plants, there has been interest in producing these compounds in metabolically engineered micro-organisms[39]. Producing high yields of precursors to opiate drugs, like the key THIQ branchpoint molecule (*S*)-reticuline allows production of high yields of downstream products including morphine and codeine using yeast as cell factories[19]. Amongst micro-organisms, brewer's yeast (*S. cerevisiae*) has garnered ample interest for THIQ production, because of its ability to express membrane localized proteins from plants (P450s)[21]. Recent work uses metabolically engineered yeast to produce improved titers of (*S*)-reticuline[23] (grams per liter). Improving (*S*)-reticuline production in yeast is a move in the direction of an alternative production method to low yielding chemical synthesis for THIQ derived drugs.

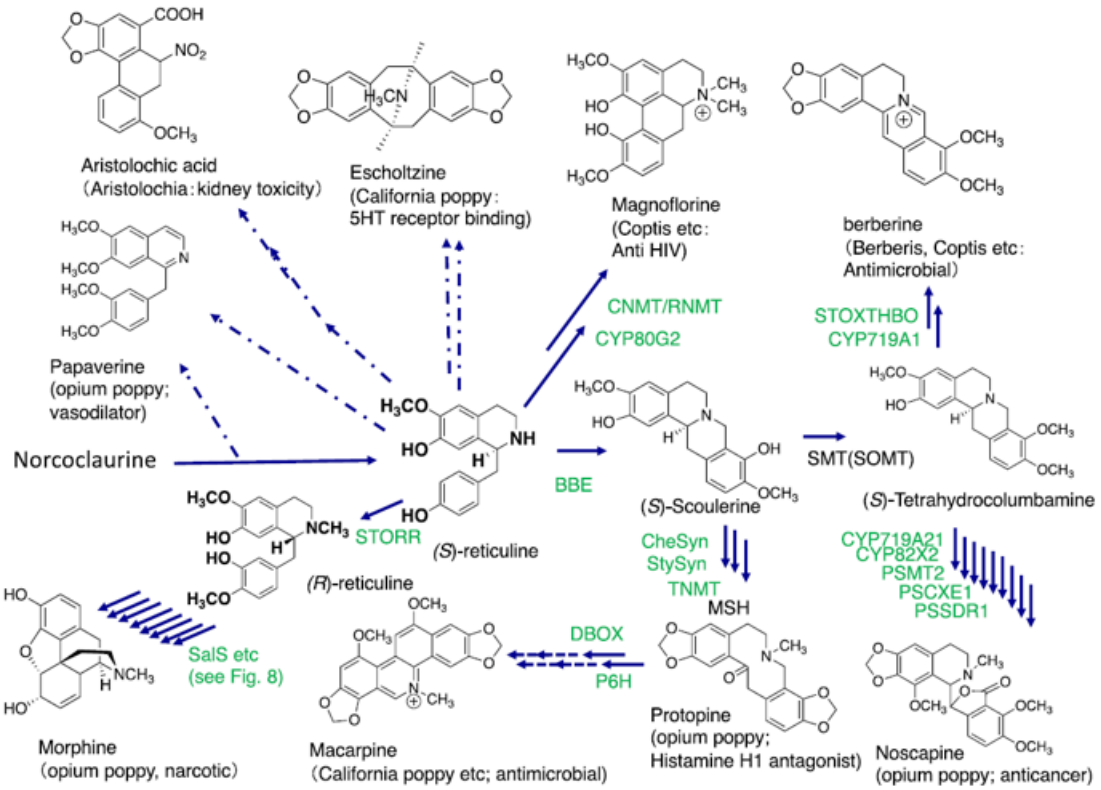

Figure 1-2. Late BIA biosynthesis derived from (*S*)-reticuline produce divergent chemicals

(*S*)-reticuline is produced from (*S*)-norcauclaurine. Molecules with a wide variety of pharmaceutical applications are produced from (*S*)-reticuline, including antimicrobials, cancer implicated molecules and narcotics. Enzyme reactions shown by dotted lines are not characterized yet at molecular level. Enzyme names are shown in abbreviations. Reproduced with permission from Elsevier Inc[40].

1.1.5 Current metabolic engineering studies related to (*S*)-reticuline production

Since elucidation of the biosynthesis pathway for opiates in the opium poppy, *P. somniferum,*[41,42] much work has gone into elucidating microbial biosynthesis pathways of these BIA compounds including (*S*)-reticuline (**Figure 1-3**). Early efforts using crude enzymes extracted from *E. coli* produced 55 mg/L (*S*)-reticuline, starting from exogenously added dopamine[43]. Using sugar as a feedstock (*de novo* production) instead of exogenous dopamine more closely resembles industrial

scale fermentation processes, including methods that use sugars as a feedstock to produce fuel[44]. To produce (*S*)-reticuline *de novo*, sufficient titers of the (*S*)-reticuline precursor dopamine are required, and to produce dopamine, high titers of the dopamine precursor L-DOPA are required. To improve (*S*)-reticuline precursor production, a fluorescent biosensor was used which converted L-DOPA to a fluorescent molecule (betaxanthin). This biosensor was used to screen a mutant library of tyrosine hydroxylase enzymes to identify variants with improved activity[25]. Yeast strains harbouring an improved tyrosine hydroxylase enzyme produced 2.8 fold higher L-DOPA titer than the wild type[25]. Introducing a Dopa Decarboxylase (DODC) enzyme allowed the first production of *de novo* dopamine by yeast[25]. The strain that produced improved L-DOPA titer also produced higher titers of the downstream metabolite dopamine[25]. Improvements in *de novo* dopamine production in yeast laid the foundation to produce BIA's in yeast. Condensation of dopamine with the yeast Ehrlich pathway intermediate 4-HPAA by Norcauclaurine Synthase (NCS) produced the BIA (*S*)-norcouclaurine[25]. The NCS enzyme has limited substrate specificity and catalyzes a second condensation reaction between a hydroxylated 4-HPAA, to produce a hydroxylated analogue of (*S*)-norcauclaurine, norlaudanosoline (**Figure 1-3**). Incorporation of 3 plant methyl transferase enzymes, a cytochrome p450 enzyme and its reductase partner allowed the complete biosynthesis of (*S*)-reticuline via (*S*)-norcauclaurine in yeast at low titers (19.2 μg/L)[45]. Using the (*S*)-reticuline biosynthesis pathway proceeding via nolaudanosoline produced fewer off-pathway THIQ's[46]. After completing the biosynthesis pathway in yeast, modifying the yeast shikimate, Ehrlich and L-tyrosine pathways improved the titer of (*S*)-reticuline to 4.6 g/L, approaching the industrial benchmark of 5 g/L[23].

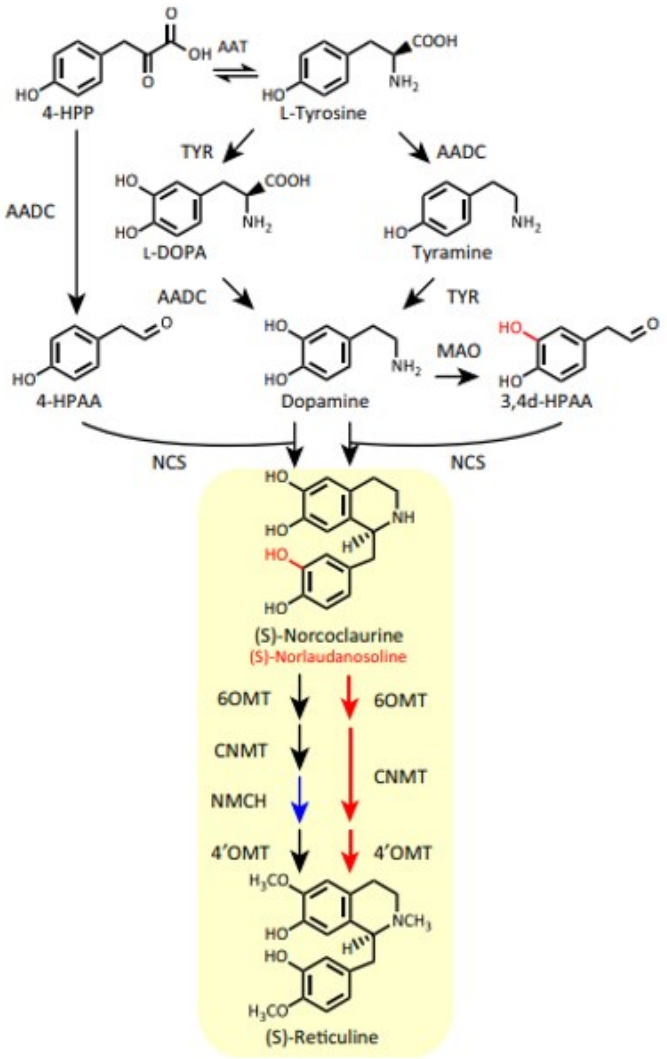

Figure 1-3 (*S*)-reticuline biosynthesis pathway in yeast.

Condensation of 4-HPAA and dopamine by NCS yields (*S*)-norcauclaurine, and through the action of 6OMT, CNMT, NMCH and 4'OMT yields (S)-reticuline. An alternative route to produce (*S*)-reticuline is the condensation of 3, 4d-HPAA with dopamine by NCS, which produces (*S*)-reticuline through 6OMT, CNMT and 4'OMT. Reproduced with permission from Cell Press[47]

1.2 High throughput screening

1.2.1 Current screening technologies for metabolite production

To measure a library of heterologous metabolite producing yeast strains, high throughput analysis methods are required. Current workflows for BIA measurement consist of spreading yeast on agar plates, growing colonies in well plates, extracting metabolites from growth medium, followed by analysis using LC/MS[23], or fluorescence[25] (**Figure 1-4**). An (*S*)-reticuline producing yeast library of $1.28*10^{37}$ variants (calculation 1-1) would take $3.65*10^{32}$ years (calculation 1-3) to screen using LC/MS. An alternative analysis approach would use a biosensor, as was done to improve L-DOPA yield[25]. This would require 911 well plates (calculation 2) to screen the library using fluorescence detection, state of the art robotics coupled to fluorescence detectors can only accommodate 50 plates[48]. Higher throughput analysis methods are required to screen this library.

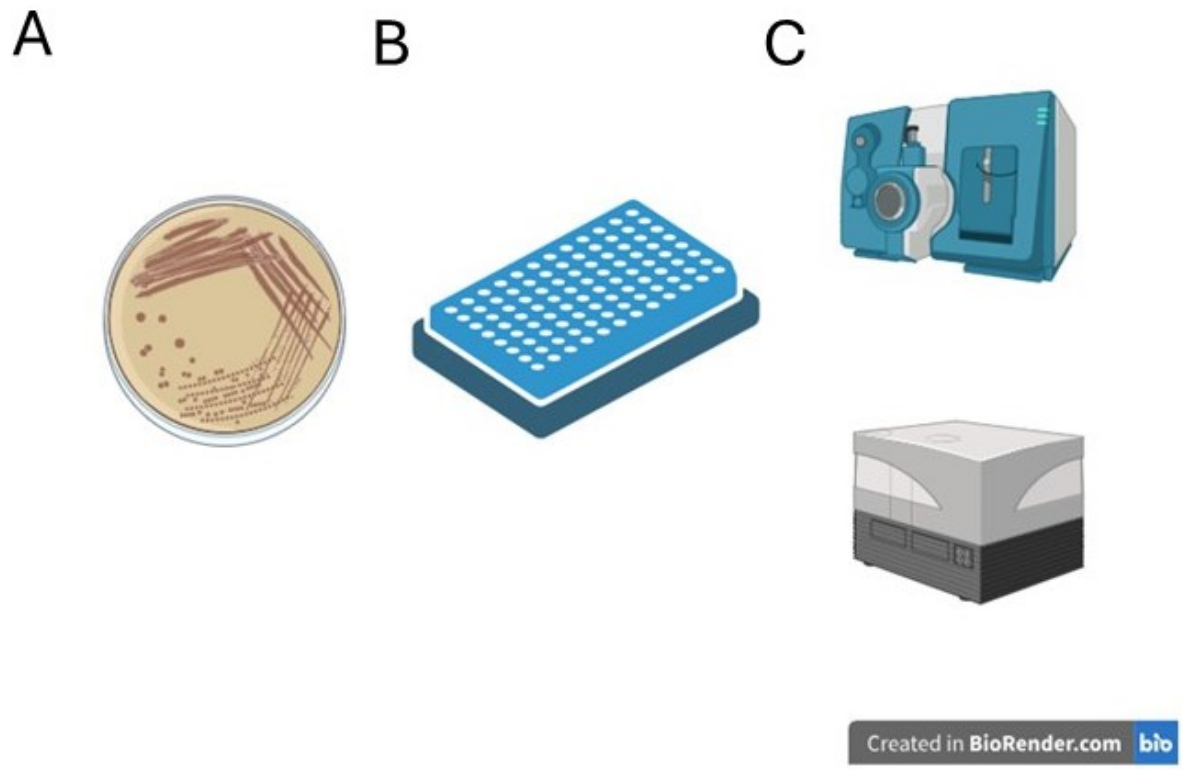

Figure 1-4 Conventional workflow for detecting heterologous yeast metabolites.

Yeast cells are streaked on a growth medium containing agar plate (A). Single yeast colonies from the agar plate are inoculated into liquid growth media in a 96 well plate, and incubated (B) Metabolites in the well plate are detected using LC/MS or fluorescent detection (C).

1.2.2 Screening large libraries for (*S*)-reticuline production

Since screening variants of a tyrosine hydroxylase enzyme in the (*S*)-reticuline biosynthesis pathway improved yields up to the precursor dopamine[25], it is expected that screening variants of the enzymes that catalyze the BIA biosynthesis reactions between dopamine and (*S*)-reticuline should further improve the yield of (S)-reticuline, if there are (*S*)-reticuline precursors accumulating in the yeast or surrounding medium that are available as reactants. Of the BIA's in the (*S*)-reticuline pathway, (*S*)-reticuline was the most abundant in the strain that produces the highest titer to date, however, that strain also produced the precursor (*S*)-norcauclaurine, which was not metabolized into (*S*)-reticuline and the BIA intermediates between (*S*)-norcauclaurine and (*S*)-reticuline were not measured. By improving the intermediate biosynthesis steps between (*S*)-norcauclaurine to (*S*)-reticuline, the (*S*)-reticuline yield could be improved further.

There are multiple methods to generate libraries of yeast with mutations in the genes encoding the biosynthesis enzymes that catalyze the reactions between dopamine and (*S*)-reticuline. One technique for mutating genes encoding biosynthesis enzymes is UV-mutagenesis[49]. UV-mutagenesis is a non-selective mutagenesis technique and leads to off-target mutations[50]. Alternatively, Chromosomal Repair Assisted Pathway Shuffling (CRAPS) allows for the generation of combinatorial libraries of yeast containing variants of multiple genes involved in heterologous biosynthesis pathways[24]. Using a library of yeast cells generated via CRAPS composed of variants of the enzymes at each biosynthetic step between dopamine to (*S*)-reticuline

is an approach to further improving the production of (*S*)-reticuline in yeast, with fewer off-target mutations. These new enzyme variants may also catalyze new reactions that create new drug candidates for pharmaceutical development. After building a library using CRAPS, testing the library to identify improved variants requires analysis tools.

1.2.3 Droplet microfluidics

Droplet microfluidics is an ultra-high throughput technology that is used to create discrete droplets of aqueous liquid that are interspersed with an oil phase, of a controlled size[51–53]. Droplet microfluidic devices use a channel design that is optimized for fluid shearing to generate droplets, such as T-junction or flow focusing geometry (**Figure 1-5**). The speed and size of droplets are dictated by the flow rates of the aqueous and oil phases[54]. Hydrophobic coatings are used to seal the channel in microfluidic devices made of PDMS[55]. The oil phase that is used in droplet microfluidics contains a surfactant – a molecule with a polar head and non-polar tail, which reduces the surface tension between the aqueous droplets and the surrounding oil, allowing the formation of stable droplets[56].

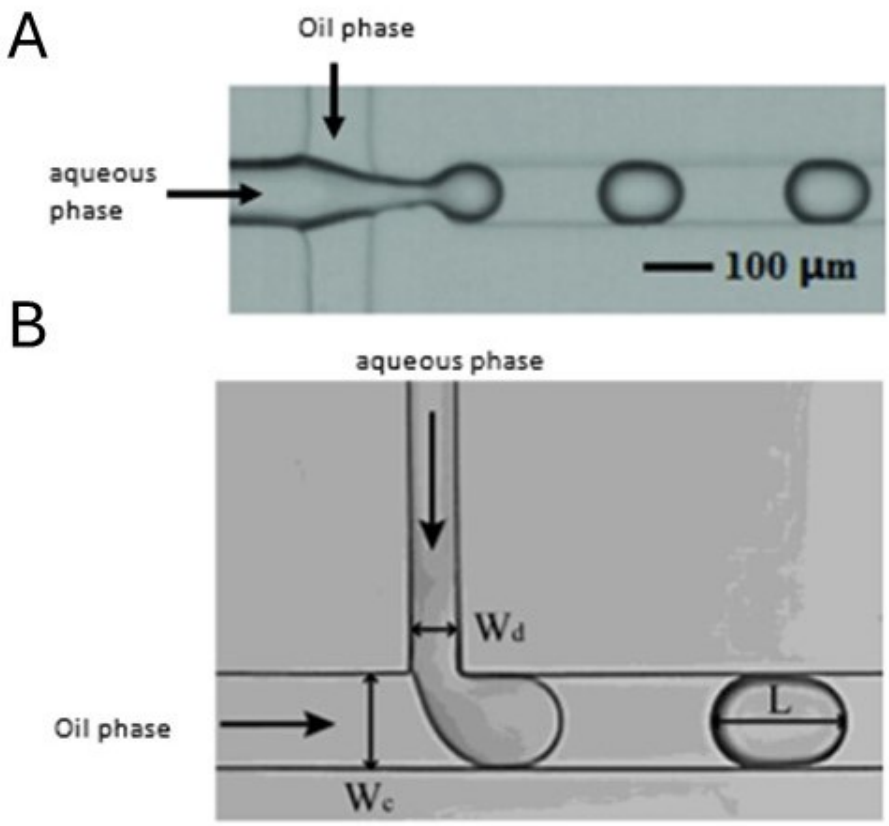

Figure 1-5 T Junction and Flow focusing droplet generators

Droplets generated using a flow focusing droplet generator, where an oil phase flowing perpendicular to the aqueous phase from two directions pinches the aqueous phase, forming droplets. Reproduced with permission from MDPI[57] (A) Droplet generated using a T-junction droplet generator, where shear forces separate an aqueous droplet as it enters the main channel of the device. Reproduced with permission from MDPI[58] (B).

Droplet microfluidics is used to compartmentalize individual reactions in droplets, allowing single molecule detection[51], and analysis of single cells[59–61]. These compartmentalized reactions provide highly accurate data, since each droplet is counted as an individual sample. Individual molecule compartmentalization is useful when highly accurate measurements are required[62], or for identifying rare cells[63]. The conventional approach for identifying rare cells in a population is fluorescence activated cell sorting (FACS), which sorts cells based on size, granularity or fluorescence[64]. FACS cannot be used when measuring secreted products, because

there is no way to couple secreted products to the cell that secreted them. Single cell compartmentalization in droplets has been used to identify cells in a population of 10,000 by their secreted metabolite production[63]. To encapsulate single cells, the cells are diluted to a concentration that maximizes the number of droplets containing a single cell. A dilution calculation is used to identify the concentration of cell that will provide the most droplets with single cells, in a probability distribution called a Poisson distribution[65]. The most common way to identify droplets in a population with the desired phenotype is using fluorescent detection[49,63].

Fluorescence activated droplet sorting (FADS) builds on droplet microfluidics and incorporates a fluorescence detector for analysis, and droplet sorter, allowing the automated isolation of droplets with high fluorescence[66]. In a FADS workflow (**Figure 1-6**), single cells are encapsulated with fluorogenic enzyme substrates in droplets. Those droplets pass by an absorbance[55,67] or fluorescence[66] detector. A threshold is applied to the signal: if the fluorescent signal is above a certain intensity, a sequential actuation of electrodes isolates that droplet to a designated outlet channel[49]. Some microfluidic device designs make use of electrodes that are coplanar: they are situated below the channel[49], while other device designs use dielectrophoretic sorters[68], with electrodes situated beside the channel. FADS sorts thousands of droplets per second, making it a very useful tool for studies that involve screening large libraries[66,67,69,70].

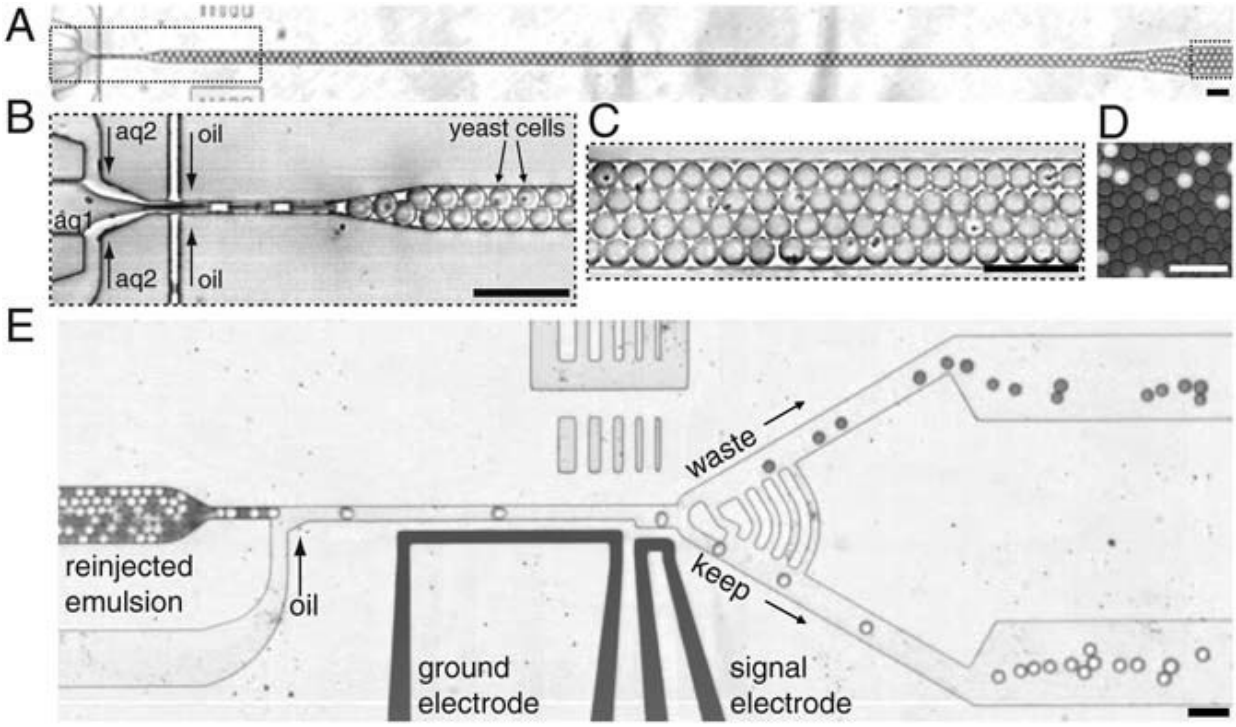

Figure 1-6 Modules of the ultrahigh-throughput microfluidic screening platform (FADS).

Droplets containing yeast, with the HRP enzyme expressed on the cell surface in aqueous stream 1 (aq1) are encapsulated in droplets with the substrate for the HRP enzyme (aq2), as seen with a low resolution image (A), and high resolution image (B). Droplets flow into an incubation area (C), where the enzymatic reaction takes place. Droplets containing yeast, which express active variants of the HRP enzyme fluoresce, while droplets containing yeast which contain inactive variants of HRP do not, leading to a heterogeneous population of droplets some fluorescent, and some not (D). The heterogeneous population of droplets are reinjected into a sorting device, where oil is used to separate droplets. Separated droplets pass by a fluorescence detector, and the fluorescence detector triggers the activation of the signal electrode, which pulls fluorescent droplets into the keep channel, when the fluorescence of a droplet passes a threshold (E) (Scale bar, 80 μm.). Reproduced with permission from PNAS[71].

Improved hydrolase enzymes isolated using FADS efficiently break down phosphate triester pesticides[72], demonstrating the utility of FADS an enzyme improvement tool. FADS is also used for screening cells based on activity of secreted enzymes[49], to identify strains with improved protein secretion[26], and for screening yeast cells by metabolite production or consumption[63]. In a FADS workflow for improved enzyme activity, the authors provided a labelled substrate, which is converted enzymatically to a fluorescent product, and sorted based on fluorescence intensity of the

product after enzymatic conversion (**Figure 1-6**). Since (*S*)-reticuline is secreted by yeast,[73,74] FADS would be an ideal screening method for an (*S*)-reticuline producing library, except that FADS sorts based on a fluorescence signal. (*S*)-reticuline isn't fluorescent, and unlike L-DOPA, there are no known products that are enzymatically converted in one step from (*S*)-reticuline to a fluorescent product. An alternative high throughput screening system for (*S*)-reticuline quantification must be used instead of fluorescence detection, such as detection using electrochemistry.

1.3 Electrochemistry

1.3.1 Electrochemistry fundamentals

1.3.1.1 Introduction to electrochemistry

Electrochemistry is the field of chemistry relating to redox reactions in which there is a transfer of electrons from one molecule to an electrode. Not all redox reactions involve electrodes, some happen in nature including the biological electron transport chain[75]. In an electrochemistry research setting, electrochemical reactions take place in a cell: a container with electrodes immersed in an ion-rich solution (electrolyte). There are two types of electrochemical cells. Galvanic cells are used as energy storage media (batteries), which release energy through spontaneous redox reactions[76]. In an electrolytic cell, an applied potential is used to drive non-spontaneous redox reactions[74]. Electrolytic cells are used for analytical purposes.

1.3.1.2 Electrochemical detection

In a cell that is used for electrochemical detection, there are three electrodes immersed in an electrolyte solution: a working electrode, reference electrode, and counter electrode. The counter electrode's role is to establish a connection to the working electrode through the electrolyte solution[77]. The reference electrode provides a reference point for the potential[75]. For this reason, the potential measured in electrochemistry experiments is denoted as potential *versus* the reference electrode used. Various materials are used as working and counter electrodes, with unique advantages. Gold electrodes are used for their good conductivity, biocompatibility and good chemical stability[78]. Carbon electrodes can be used for measurements over a wide range of potentials (potential window)[79]. One type of carbon electrodes are carbon paste electrodes, which can be moulded using screen printing techniques[80–82]. A critical criterion for selecting a working electrode material is the ability of the working electrode to detect the analyte of interest[83].

When a molecule is in reduced form, and that molecule's experimentally determined standard oxidation potential is applied, electrons are transferred from that molecule to the electrode, either directly, or through an electron transfer intermediate[84], leaving the molecule in oxidized form. For example, applying the standard oxidation potential of copper (+0.342 V versus standard hydrogen reference electrode) oxidizes it to Cu^{2+}, releasing two electrons (**Figure 1-7**), and vice versa for reduction. Since different molecules have different oxidation and reduction potentials, applying specific potentials can be used to selectively oxidize or reduce molecules in a heterogeneous solution, including biological samples[85]. Asides from the electron transport chain[75], there are other biological redox reactions that are catalyzed by oxidoreductase enzymes. One such enzyme is the Berberine Bridge Enzyme, which catalyzes the oxidation of (*S*)-reticuline to form

(*S*)-scoulerine (**Figure 1-8**). Reactants in biological redox reactions are candidates for electrochemical detection, since it is known that they participate in redox reactions.

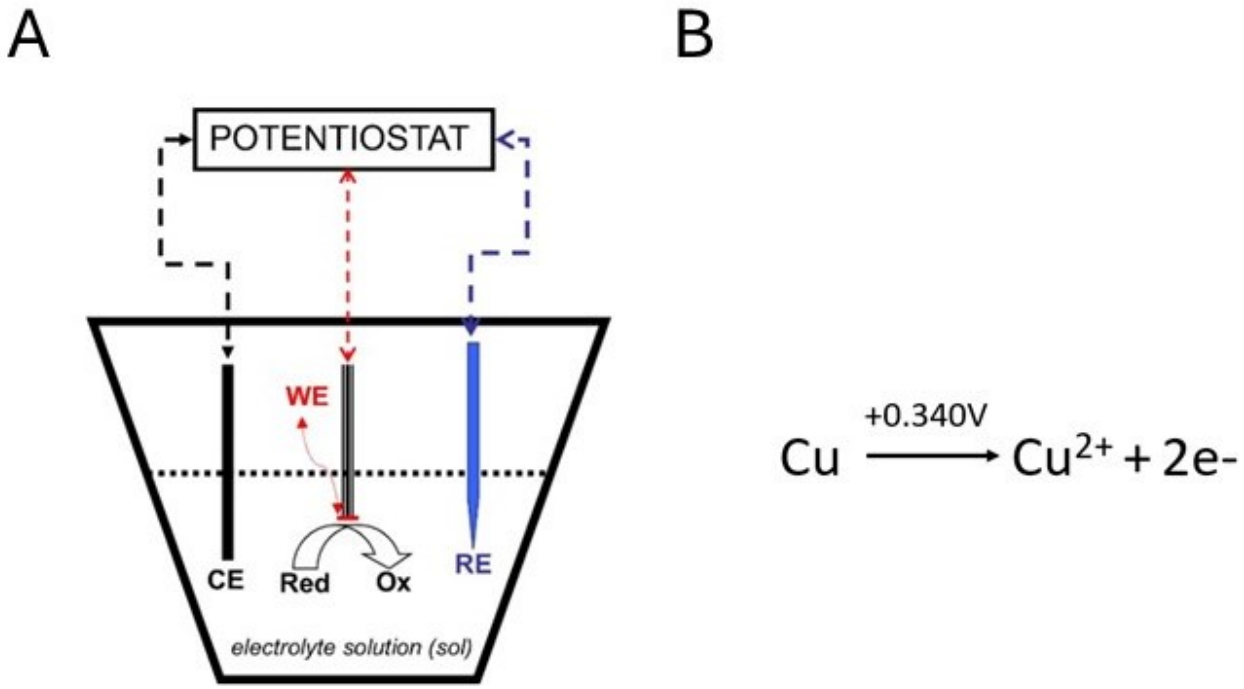

Figure 1-7 Electrochemical redox reactions

When a potential is applied between the working and reference electrode in an electrochemical cell, oxidation or reduction reactions happen at the working electrode if the applied potential is the oxidation or reduction potential of analytes in the cell (A). An example redox reaction, the oxidation reaction of metallic copper to Cu^{2+} happens when the standard oxidation of copper is applied[86] (B). CE is counter electrode, WE is working electrode, RE is reference electrode. Red is a molecule in reduced form, Ox is a molecule in oxidized form. Reproduced with permission from Springer[87].

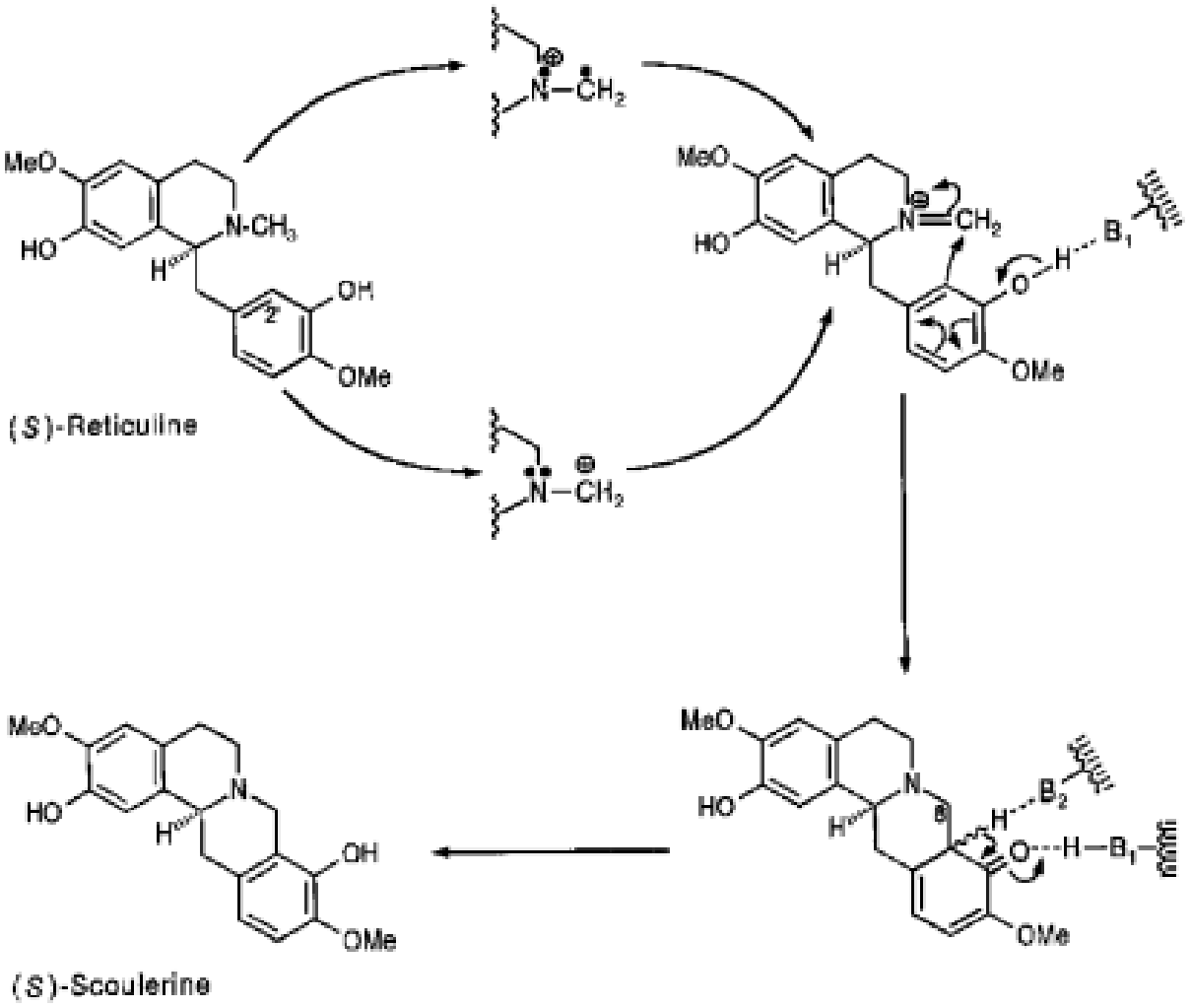

Figure 1-8 - Proposed mechanism of enzymatic (*S*)-reticuline oxidation

The oxidative cyclization of (*S*)-reticuline to (*S*)-scoulerine proceeds via a two step mechanism: oxidation to the methylene iminium ion followed by nucleophilic attack at the imine carbon by C-29 to form C-8, the berberine bridge. B1 and B2 are proposed basic residues of the enzyme involved in semiquinone formation and aromatization, respectively. Reproduced with permission from The American Society for Biochemistry and Molecular Biology[88].

1.3.1.3 Electrochemical analysis

The electrons that are generated by oxidation or reduction reactions are measured as current. This current generated by redox reactions is known as faradaic current[77], while current generated by the accumulation of ions at the electrode surface is referred to as capacitive current[77]. For example,

the oxidation of metallic copper produces two electrons (**Figure 1-7**), which are measured at the working electrode as faradaic current. The more reduced form of the molecule of interest is present when the standard oxidation potential is applied, the more current is generated in the oxidation reaction. The current generated in the reaction is measured by a potentiostat (**Figure 1-7**).

Since the current generated in redox reactions is proportional to the amount of reactant that is present, electrochemistry can be used as an analytical tool. This field of electrochemistry is called electroanalysis. Electroanalysis uses a variety of techniques to measure analytes in solution. Voltammetry is a category of electrochemical measurement where current is measured during a potential sweep,[89] and includes the analytical techniques cyclic voltammetry (CV) and differential pulse voltammetry (DPV). Voltammetry techniques are commonly used for sensor development[85,85,90–93] because they allow the selective determination of analytes that oxidize or reduce at different potentials. Amperometry is a category of electrochemical measurement, where a fixed potential is applied, and current is measured[94], and includes chronoamperometry (CA). CA is used for electrochemical measurement in droplets[68,82,91,95–97].

1.3.2 Electrochemical Analysis Techniques

1.3.2.1 Cyclic voltammetry

Cyclic voltammetry (CV) is an electrochemical technique which measures current generated by the oxidation and reduction of an analyte in solution[77]. In cyclic voltammetry, a linear sweep of potential is applied by increasing the potential in the forward scan until the potential reaches a switching potential, at which point the potential is decreased. (**Figure 1-9**). Both the increase and decrease of the potential in cyclic voltammetry are linear. According to the Randles–Ševčík

equation (equation 2), when a measurement is taken using an electrode of a fixed size, with a solution containing an analyte with a fixed diffusion coefficient in an electrolyte, and the scan rate is held constant, the concentration of the analyte in the electrolyte is proportional to the peak height. This relationship between peak height and concentration allows voltametric analysis techniques to be used for quantification of analyte in solution. CV produces an oxidation peak and a reduction peak on a voltammogram: a plot of current vs potential (**Figure 1-9**). The oxidation peak current ($I_{p,a}$) is used to measure the oxidation of the analyte in solution, while the reduction peak current ($I_{p,c}$) is used to measure the reduction[77]. CV is useful for characterization experiments to find out if a molecule will oxidize or reduce using a particular working electrode, and at what potential the molecule will oxidize ($E_{p,a}$) and reduce ($E_{p,c}$) at. A drawback of CV is that it is not very sensitive due to high capacitive current[98].

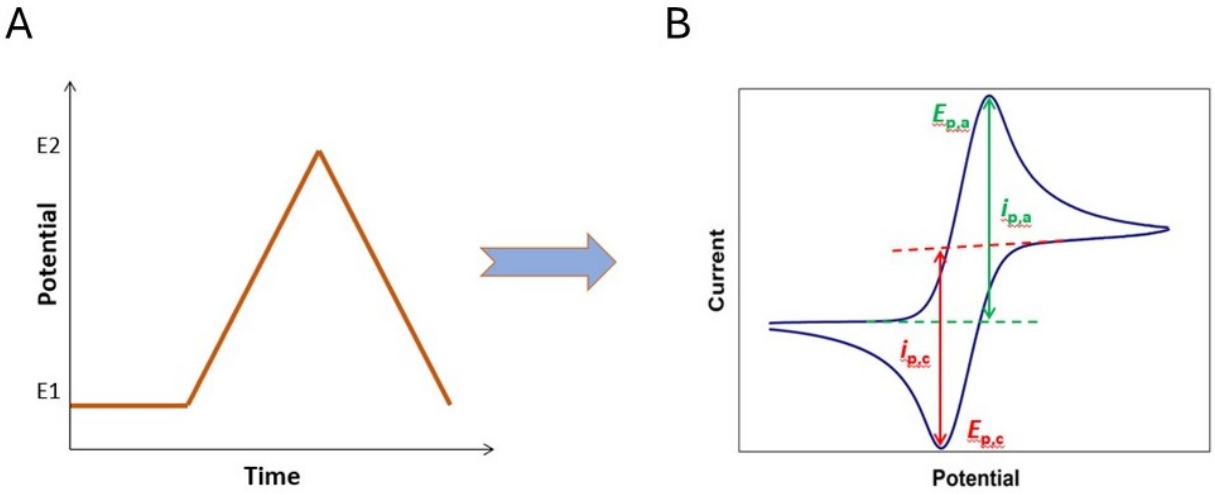

Figure 1-9 Cyclic voltammetry

The potential waveform applied in cyclic voltammetry sweeps positively from a low potential (E1) to a high potential (E2) and then sweeps negatively from E2 to E1 (A). The resulting voltammogram has an oxidation peak of current ($I_{p,a}$) at the peak potential ($E_{p,a}$) in the positive sweep, and a reduction peak of current ($I_{p,c}$)at the reduction potential ($E_{p,c}$) (B). Images courtesy of Dr. Kekedy-Nagy.

1.3.2.2 Differential pulse voltammetry

Differential pulse voltammetry (DPV) is another voltammetry technique, which is used for electrochemical analysis. DPV applies a stepwise potential over time waveform (**Figure 1-10**). By measuring current generated throughout potential pulses, DPV minimizes the capacitive (background) current. For this reason DPV is a more sensitive analytical technique than CV[99]. Like CV, DPV applies a potential sweep. That potential sweep takes time (seconds to minutes), and each potential sweep can only be used to take a single measurement, so it is not an ideal technique for high throughput measurements.

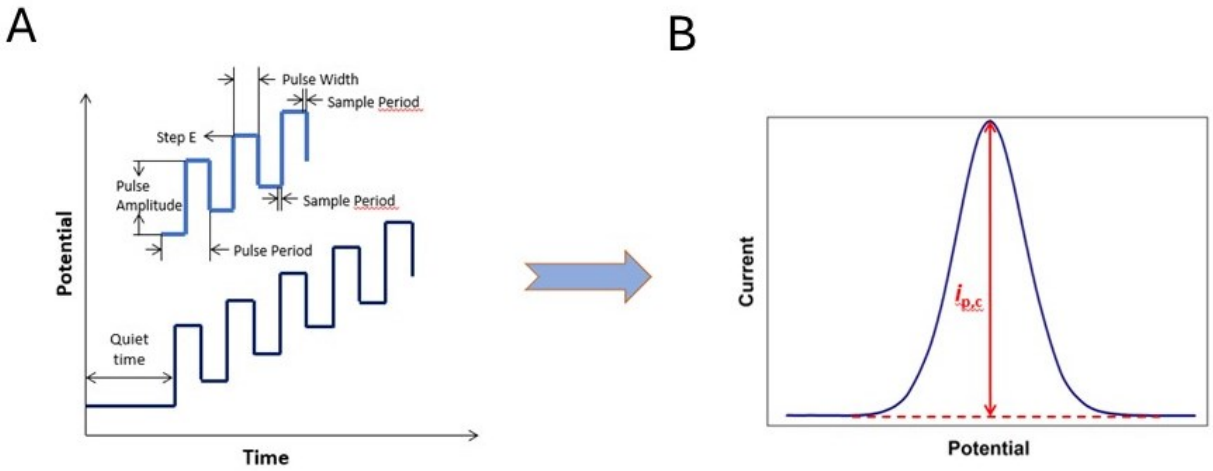

Figure 1-10 Differential pulse voltammetry

The applied potential waveform in differential pulse voltammetry has an overall trend of increasing potential, with potential pulses which increase immediately, are held constant, then decrease immediately. This potential waveform (A) allows the subtraction of capacitive current from the faradaic current, which can not be done using a linear potential sweep, like cyclic voltammetry. A DPV oxidation voltammogram shows a positive current peak at the oxidation potential (B), $I_{p,c}$ is peak current. Images courtesy of Dr. Kekedy-Nagy.

1.3.2.3 Chronoamperometry

Chronoamperometry (CA) is an electrochemical analytical technique, where a constant potential is applied, and current is measured over time (**Figure 1-11**). In chronoamperometry experiments, an exponential decrease or increase of the current is observed as the analyte is consumed, depending on whether the analyte is oxidized or reduced (**Figure 1-11**). The Cottrell equation (equation 1) describes this change in current over time when a constant potential is applied[62].

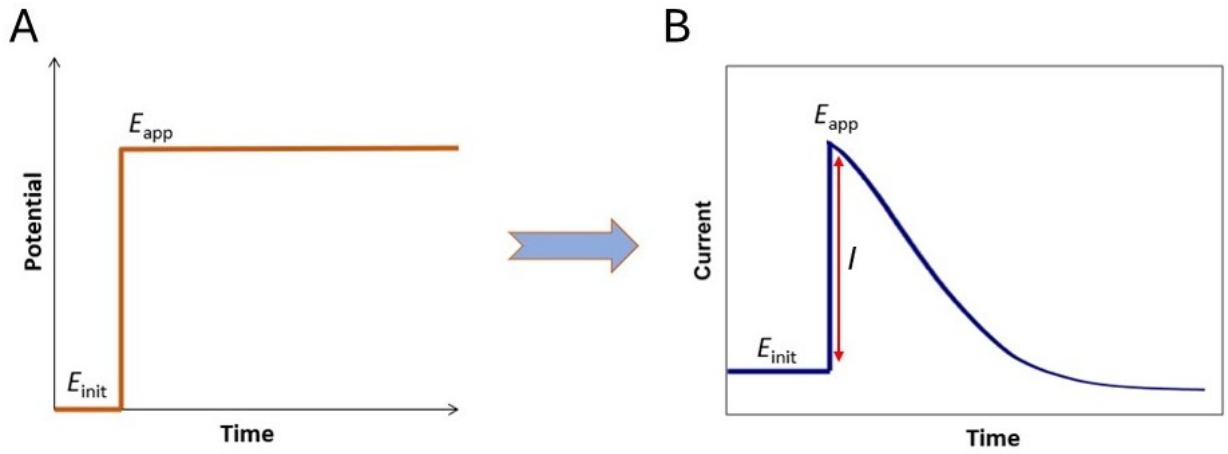

Figure 1-11 Chronoamperometry
A fixed potential is applied (A), and current (I) is generated upon the application of potential (B). The current decays as the analyte is consumed in the reaction. E_{init} is initial potential, E_{app} is applied potential

Table 1-1: Electroanalysis techniques used in sensor development and high throughput analysis

Technique	Advantages	Disadvantages	Application
Cyclic Voltammetry	oxidation and reduction in a single measurement	low sensitivity, low throughput	identification of oxidation and reduction peaks i.e. initial characterization in sensor development studies[81,100]
Differential Pulse Voltammetry	high sensitivity	low throughput	sensitive, quantitative measurement, i.e. diagnostics[90,92,101]
Chronoamperometry	high throughput	low sensitivity	measuring droplet contents[82,96,97] i.e. screening experiments[68]

1.3.3 Electrochemistry integrated with microfluidics

Microfluidics has been integrated with electrochemical detection for applications including disease diagnostics and assessment, as well as high throughput detection of pharmaceutical compounds. In a work investigating metabolites produced by single cancer cells, a capillary injection and aspiration tube (push-pull nozzle system) (**Figure 1-12a**) was used to deliver glucose to single cells, measuring lactate production[102] which is used for cancer diagnosis[103]. This sensor used an oxidoreductase enzyme (lactate oxidase) to selectively detect lactate by oxidizing it to pyruvate in the presence of other biological media. Using this system, they were able to distinguish between the current responses of lactate produced by cells which were fed glucose through their push-pull nozzle system, showing promise for this device as a method to investigate the metabolism of cancer at the single cell level. A complimentary approach to using enzymes for selectively measuring analytes in complex media is to incorporate a purification process on the device. Incorporating purification processes on diagnostic devices is an approach that is used to separate components that contain diagnostic data from complex biological samples. After purifying extracellular vesicles (EV's), from patient samples, another group were able to detect cancer specific surface markers on tumour derived EV's (**Figure 1-12b**).

For real time measurement of metabolites in human sweat, wearable sensors are used. By incorporating the conductive polymer PEDOT:PSS in a wearable sensor with a carbon electrode (**Figure 1-12c**), Xu et al. overcame the challenge of mechanical stability (fragility) in one microfluidic electrochemical system[104]. Measuring uric acid in sweat using this PEDOT:PSS carbon electrode system allowed them to assess the risk of gout and hyperuricemia.

Other work integrating electrochemical sensors with microfluidics aims to develop high throughput analysis systems. Using a two-layer PDMS device, with screen printed carbon paste-PDMS electrodes in one layer, and a droplet generator with a confined channel in the other layer Suea-Ngam et al. was able to detect dopamine analytical standard in droplets, by distinguishing increased current peak height with increasing concentrations in droplets (**Figure 1-12d**). The integration of electrochemical sensors with microfluidic devices has been used to detect metabolites in biological samples using selective, but using low throughput analysis systems. High throughput analysis systems have been used to detect analytical standards. There is a lack of literature using electrochemical measurement integrated with droplet microfluidics for high throughput measurement in biological samples.

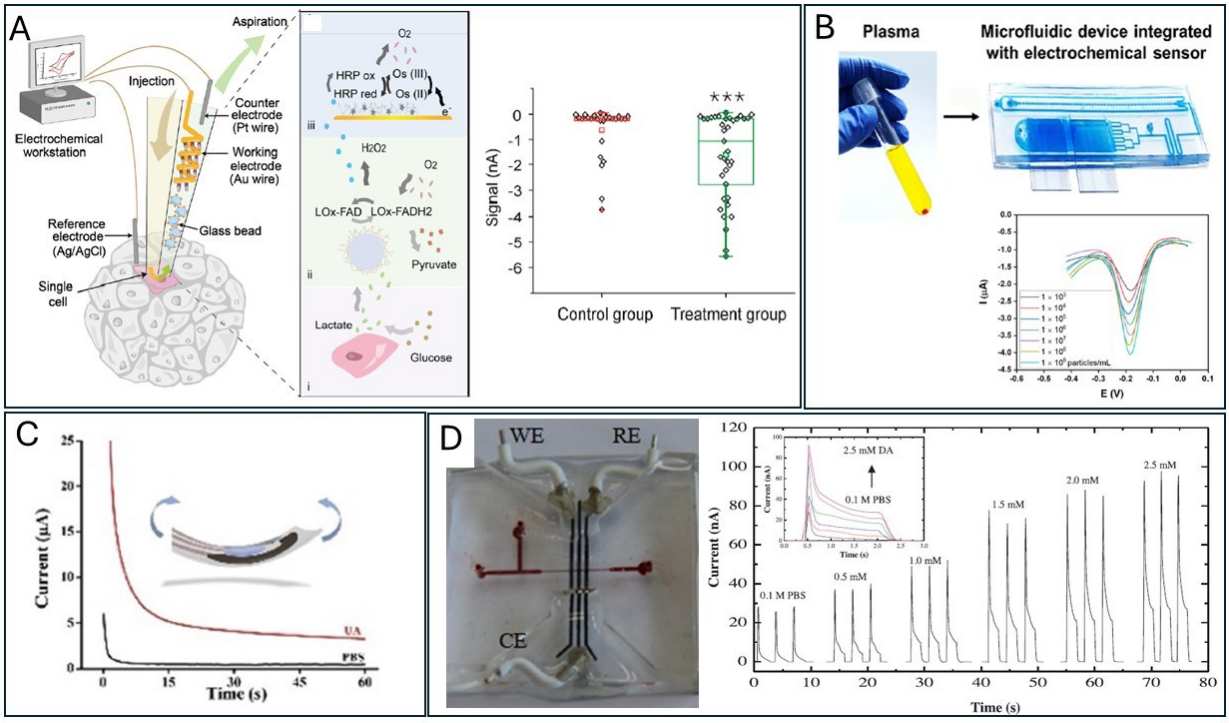

Figure 1-12 Electrochemical detection integrated with microfluidics

Enzymatic electrochemical sensors (A) and integrated separation techniques (B) demonstrate two approaches to selective detection of metabolites in biological samples on microfluidic devices integrated with electrochemical sensors. Building electrochemical sensors using flexible materials is one approach to

maintaining mechanical integrity of miniaturized carbon sensors (C). Carbon paste-PDMS electrodes can be integrated with droplet microfluidic devices to detect pharmaceuticals using chronoamperometry. WE is working electrode, CE is counter electrode, RE is reference electrode (D). Reproduced with permission from ACS Publications (A)[102], Biosensors and Bioelectronics (B)[100], Sensors and Actuators B: Chemical (C)[105] and Analytica Chimica Acta (D)[82]

1.4 Thesis objectives

The main goal of my project is to develop a high throughput method for detecting electroactive secreted metabolites produced by engineered micro-organisms, as a tool to use in the test step of the metabolic engineering cycle. As a model system for our work, we used engineered yeast cells that has been modified to produce (*S*)-reticuline. The approach taken is to develop a system like FADS, however, I will develop an electrochemical method instead of fluorescence detection. This electrochemically activated droplet sorting system (which we call "EADS") selectively measures metabolite (in our case (*S*)-reticuline) produced by yeast, and isolates droplets containing the highest (*S*)-reticuline producing variants (**Figure 1-13**). Demonstrating that this screening system works for improved production of (*S*)-reticuline opens the possibility of using EADS to screen libraries of metabolically engineered microbes that produce other valuable non-fluorescent metabolites.

To work towards this goal, I have divided my work into four specific aims: (1) to measure (*S*)-reticuline standards using a traditional electrochemical cell (i.e. bulk-scale measurements), (2) designing and characterizing an electrochemical sensor that can be integrated with a droplet-based microfluidic device, (3) investigating the selectivity of the sensor for (*S*)-reticuline in the presence of other BIA's and yeast metabolites, and (4) measuring the desired metabolite in yeast culture and sorting the desired yeast variants that produce the metabolite of interest.

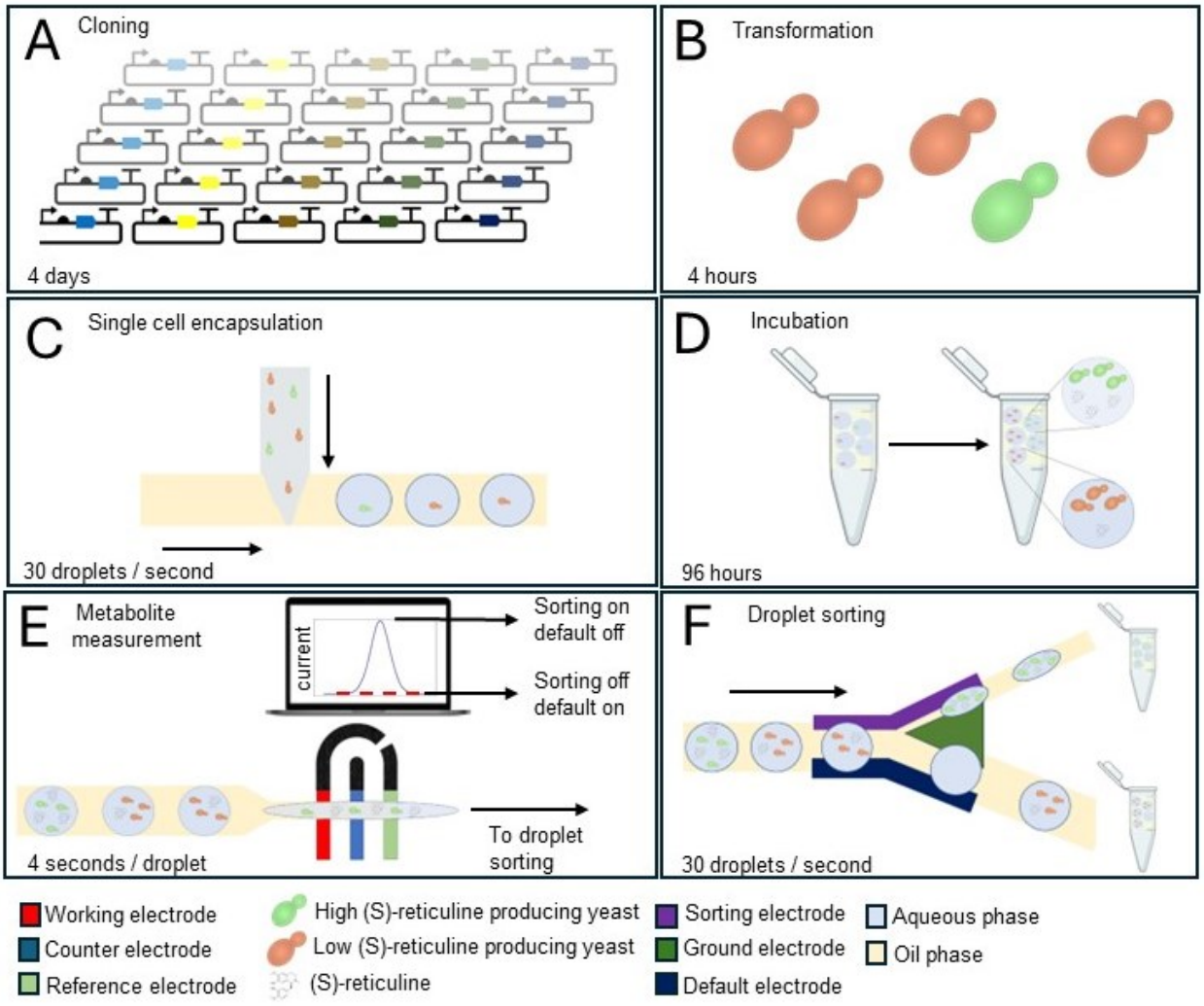

Figure 1-13 Electrochemically activated droplet sorting

Combinatorial assembly techniques are used to assemble DNA parts (A) Parts are transformed into cells (B) Single yeast cells are encapsulated in droplets: aqueous electrolyte solution containing a heterogeneous yeast culture, including some yeast cells that produce high titers of (*S*)-reticuline, and some that produce low titers of (*S*)-reticuline flow from the top facing inlet, while fluorinated oil flows from the left facing inlet (C). Incubation: yeast cells divide and secrete (*S*)-reticuline into the surrounding droplet (D). Measurement using Cr-CPE: Current measured at the carbon paste electrodes passes through the chromium wires, to the potentiostat, which records CV, DPV and CA data. The data is sent to a program, which turns on the sorting electrode, and turns the default electrode off when the current passes a threshold. When the current does not pass this threshold, the sorting electrode is off, and the default electrode is on (E). Sorting: droplets containing high (*S*)-reticuline producing yeast are isolated to the upper channel by actuating the sorting electrode, while empty droplets and droplets containing low (*S*)-reticuline producing yeast flow to the lower channel, as the default electrode is on unless the sorting electrode is actuated. This process takes 65 days to screen a library of 1,400,000 droplets containing populations derived from single cells (F). Clip art produced using BioRender.

Chapter 2

Materials and Methods

In this chapter, I will describe the methodology behind the electrochemical measurements using the bulk scale electrochemical cell, and the developed sensor. I will also elucidate the methodology used to fabricate the microfluidic devices, and describe the methodology used for graphical analysis and yeast culturing.

2.1 Reagents and materials

Acetone, potassium ferricyanide, chlorotrimethylsilane, acetone, yeast nitrogen base (YNB) without amino acids, ferrocene methanol, drop-out medium supplements, perfluorodecalin, 1H,1H,2H,2H-perfluoro-1-octanol, and dopamine hydrochloride were all purchased from Sigma-Aldrich (Oakville, ON, CA). Isopropyl alcohol (IPA) 99% was purchased from Greenfield Global (Boucherville, QC, CA). The phosphate buffered saline (PBS, 1X, Multicell, without calcium and magnesium) was purchased from Wisent Bioproducts (St-Bruno, QC, CA), while (*S*)-reticuline was purchased from Cedarlane Labs (Burlington, ON, CA). Yeast strains LN1069, LP507, GC1373 and BY4741 were generously donated from Dr. Vincent Martin's lab. Alumina powder 1 micron was purchased from BASi Research Products (West Lafayette, IN). Copper tape 3M 158399-ND was purchased from DigiKey (Thief River Falls, MN). Polypropylene Masterblock 96 well plates were purchased from Greiner Bio-One (Kremsmunster, Austria). LC/MS grade

acetonitrile A955-4 was purchased from Fischer Scientific (Ottawa, ON CA). Fluka 98% Formic Acid was purchased from VWR International (Mississauga, ON, CA). LC/MS grade water was purchased from Thermo Fischer Scientific (Saint Laurent, QC, CA).

Fabrication materials for droplet-digital microfluidic devices include CR-4 chromium etchant (OM Group, Cleveland, OH, USA), S-1811 positive photoresist coated glass slides (Telic, Valencia, CA, USA), MF321 developer (Rohm and Haas, Marlborough, MA, USA), <100> Si wafers (Silicon valley Microelectronics Inc., Santa Clara, CA, USA), and SU-8 5, SU-8 2035, SU-8 developer (Westborough, MA, USA). Polydimethylsiloxane (PDMS) was purchased from Krayden Inc. (Westminster, CO, USA) and chlorotrimethylsilane from Sigma-Aldrich (Oakville, ON, CA).

Microposit MF321 developer was purchased from Rohm and Haas (Marlborough, MA). Gold etchant TFA and chromium etchant 9051 were purchased from Transene (Danvers, MA, USA).The AZ300T stripper was purchased from AZ Electronic Materials (Somerville, NJ, USA), while SU8-5, SU8-2035 photoresists were purchased from Kayaku (Westborough, MA, USA). SU8 developer was purchased from Microchem (Westborough, MA, USA) and silver epoxy from MG Chemicals 8331D was purchased from Amazon.ca. Tergeo Plasma cleaner was purchased from Pie Scientific (Union City, CA, USA). Novec 1720 hydrophobic coating was purchased from 3M (Montreal, QC, Canada). Tygon ® tubing with inside diameter of 0.020 inches and outside diameter of 0.060 inches was purchased from DigiKey Canada (Concord, ON, Canada). BD Plastipak ™ 3 mL Syringes with Luer Lock tips were purchased from VWR (Montreal, QC, Canada). 25 gauge ½ inch polypropylene and stainless steel dispensing tips were purchased from McMaster-Carr (Robbinsville, NJ, USA).

2.2 Sensor and device fabrication

Au and Cr- electrode based sensors were fabricated at the cleanroom facility at Concordia University using photomasks printed at 25 400 dpi (Artnet Pro, Bandon, OR). The sensors consisted of a glass substrate coated with 100 nm gold adhered to a seed chromium layer (≈12 nm). Exposure of mask features onto the chip and all subsequent exposures were performed by the UV-KUB 3 (Kloe, FR) at 100% intensity for 7 seconds. The devices were developed using Microposit MF321 (2 min), washed with DI water, dried with nitrogen, and heated at 115 °C (1 min). Subsequently, the chips were submerged in gold etchant (2 min), washed with DI water, and submerged in chromium etchant diluted 1:1 with DI water (2 min) before rinsing with DI water again. Finally, they were placed in AZ stripper to remove the remaining photoresist before being washed with acetone, IPA, and DI water, and dried with nitrogen. Chromium electrode fabrication followed the same steps except the use of chromium etchant instead of gold etchant.

Some sensor devices were modified such that the Au- electrodes were replaced with carbon paste. Briefly, carbon paste sensor electrodes were deposited based on a previously reported method[82] in which graphite, mineral oil and PDMS elastomer were mixed at a ratio of 2:1:1 w/w/w respectively by stirring in a weigh boat, for 5 minutes. Briefly, carbon paste-PDMS mixture was applied to the surface of the SU-8 apertures (above the Cr electrodes) until the SU-8 apertures were covered. Excess carbon paste was then removed by moving a glass slide across the SU-8 apertures in the same motion that a squeegee is used in screen printing applications. This motion removed carbon paste which was not inside the SU-8 apertures. This process was repeated until the SU8 apertures were filled with carbon paste and excess carbon paste outside of the SU8 windows had been removed (**Figure 2-1**). This selective filling of the SU8 apertures with carbon paste was confirmed by visual inspection using an Olympus BX41 microscope at 4x magnification.

Connection to the potentiostat was established via applying copper tape to the contact pads and layer of Scotch tape (Magic) on top of the copper tape.

Patterned sensors were spin-coated with a 100 µm SU8-2035 photoresist layer (500 rpm at 500 rpm/s acceleration for 10 seconds, 1250 rpm at 300 rpm/s for 30 seconds. SU-8 2035 was soft-baked at 55 °C (5 min), 95 °C (20 min), exposed at 100% intensity (7 s) under the SU-8 window mask. Subsequently, a post-exposure bake was performed at 55 °C (5 min), 95 °C (20 min), cooled to room temperature (5 min). Subsequently, the Au-devices were spin-coated with a 7 µm SU8-5 photoresist layer (500 rpm at 500 rpm/s acceleration for 10 seconds, 2000 rpm at 415 rpm/s for 90 seconds, 5000 rpm at 400 rpm/s acceleration for 5 seconds, and 500rpm at 415 rpm/s for 5 seconds). SU-8 2035 was soft-baked at 55 °C (2 min), 75 °C (2 min), 95 °C (15 min), 75 °C (2 min) 55 °C (2 min) and then exposed at 100% intensity (7 s) under the SU-8 window mask. Subsequently, a post-exposure bake was performed at 55 °C (2 min), 75 °C, (2 min), 95 °C (15 min), 75 °C (2 min), and 55 °C (2 min). This was followed by immersing in SU-8 developer (1 min 45 seconds). Chips were then rinsed with IPA and dried at 55 °C (10 min) upon which a final hard bake step was performed by ramping up to 180 °C (25 min) and then baking at 180 °C (10 min).

For the channel layer, a soft-lithography procedure was followed as previously described[49]. Primarily, Si-wafers were placed under plasma oxygen for 45 s and then spin coated with 100 µm SU-8 2035 (500 rpm at 500 rpm/s acceleration for 10 seconds, 1250 rpm at 300 rpm/s for 30 seconds). The wafer was then soft baked at 65 °C (5 min) and 95 °C (20 min), then cooled to room temperature (5 min). Upon soft baking, the wafers were exposed at 100% intensity (7s). Wafers were post-exposure baked at 65 °C (13 min) and 95 °C (20 min). After the post-exposure bake, the wafers were developed in SU-8 developer for 3 minutes. The master mold was treated with

chlorotrimethylsilane vapor deposition in a desiccator (30 min). PDMS (1:10 w/w ratio curing agent to prepolymer), was poured over the mold and left to cure in an oven at 65 °C for 2 h. Inlets and outlets were made using 1.5 mm biopsy punchers (World Precision Instruments, FL, USA), fitting 0.060″ OD tubing, after which the PDMS was carefully cleaned with tape to remove debris before device assembly.

To bond the sensor electrodes to a channel layer for droplet measurements, the electrodes were covered with tape, then the device was placed in a vacuum chamber, and exposed to APTES using vapour deposition (30 min). The PDMS slabs were treated with oxygen plasma (15 s) and directly aligned with the electrodes under a dissecting microscope. The covering was removed, the PDMS channel layer was placed on top of the electrode layer, and the devices were baked at 80°C (30 mins) (Figure 2-1). Images of the devices were carried out using a Phenom ProX desktop SEM machine or using a confocal microscope to check electrode deposition and wired connections. For SEM, magnification was 1600x, and the detection type was backscattered electron analysis.

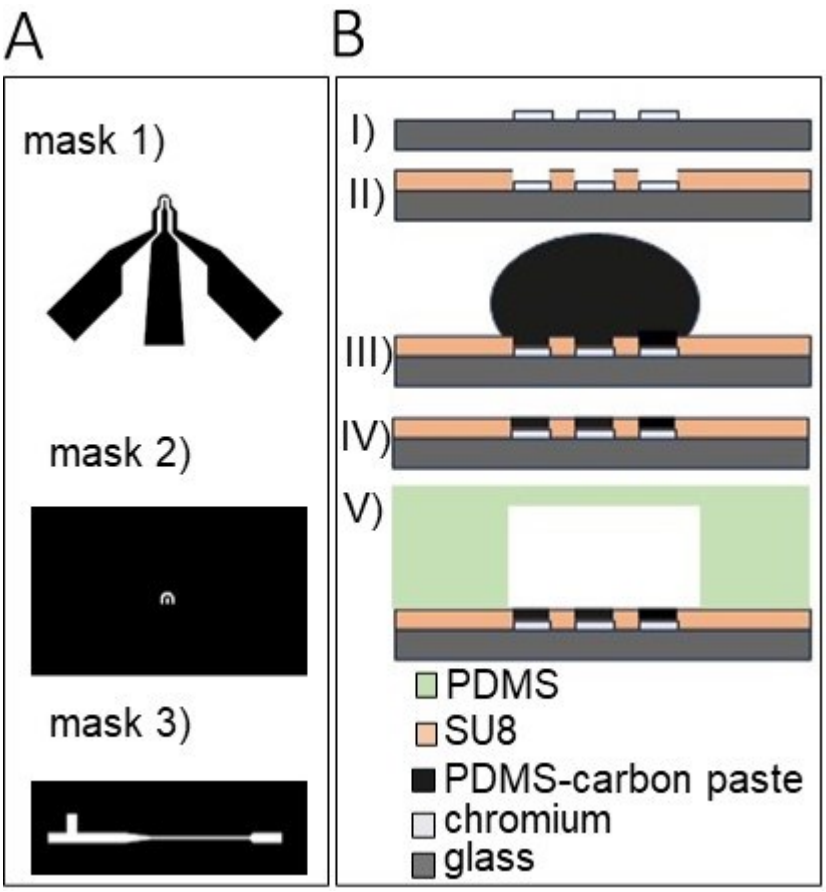

Figure 2-1 Fabrication of sensor electrodes

Masks used for device fabrication (A). Mask 1) is used for the fabrication of the chromium wire layer using photolithography, which allow contact between the carbon paste electrodes and the potentiostat. Mask 2) is used for patterning SU8 on top of the chromium wire layer. Using photolithography, the SU8 is selectively patterned to create apertures for screen printing, while insulating the chromium wires. Mask 3) is used to create a SU8 mold of the channel layer, which consists of a T-junction droplet generator, a squeezing channel for elongating droplets, to cover the entire surface of the electrodes, and an outlet for droplet collection. Fabrication process for integrating Cr-CPE with droplet microfluidics (B). Chromium electrodes are patterned on the glass substrate in step I). SU-8 is selectively patterned to expose chromium wires, leaving a 100 μm well above each wire in step II). PDMS-carbon paste is applied to the surface, filling the wells in step III). Excess PDMS-carbon paste is removed by screen printing in step IV). PDMS replica containing the channel layer is bonded on top of the sensor in step V).

2.3 Macroscale voltammetry measurements

Cyclic voltammetry (CV) and differential pulse voltammetry (DPV) were carried out in a conventional electrochemical cell with a PalmSens 4 electrochemical system (PalmSens B.V., Houten, the Netherlands) equipped with PSTrace 5 (v 5.8). The cell was comprised of a 3.0 mm diameter glassy carbon (GC) working electrode, a Ag/AgCl reference electrode with 3 M KCl internal electrolyte, and platinum coil counter electrode all obtained from BASi Research Products. For all measurements, PBS was used as the supporting electrolyte (80 mL).

(*S*)-reticuline standard was dissolved in 1M HCl to form a 15 mM stock solution. This stock solution was diluted in PBS to create a 1 mM working solution. Similarly, a 100 mM stock solution of dopamine hydrocholoride in PBS was diluted serially to create a 1 mM working solution of dopamine. 80 µL of the dopamine working solution was added to the electrochemical cell to create 1 µM solution in the cell, and 80 µL was added to create a final concentration of 9 µM dopamine in PBS. The same dilutions were made for (*S*)-reticuline to generate 2,4,6,8,10 µM concentrations using the working solution for the reticuline standard curves. A stir bar in the cell was spun for 30 seconds at 1500 rpm to ensure even dissolution of the analyte in the electrochemical cell. Prior to measurements, electrodes were cleaned by using a cloth pad was placed in the bottom of an 8 cm diameter petri dish. Alumina slurry was poured on top of the cloth pad. The glassy carbon electrodes were moved in a figure 8 shape through the alumina slurry to ensure even exposure of the electrode surface. For DPV measurements, the modulation amplitude was 40 mV with a step potential of 10 mV and a scan rate was 20 $mV \cdot s^{-1}$. In CV measurements, the step potential was 10 mV and the scan rate was 20 $mV \cdot s^{-1}$.

2.4 Device Assembly and Operation

Electrochemical sensors were cleaned, and voltametric measurements were made using the PalmSens 4 connected through alligator clips to 3M copper tape, which was connected to the chromium wires on the device. For droplet-based devices integrated with our electrochemical sensor, holes were punched forming two inlets and an outlet of the device using a 1.5 mm biopsy puncher. After hole punching, the outlet of the device was covered using Scotch (Magic) tape. 20 µL of Novec 1720 hydrophobic coating was injected into one of the inlets of the device, and exited the device through the other inlet. This selectively coated the droplet generator of the device, while preventing exposure of the electrodes to the hydrophobic coating. The devices were left at room temperature for 10 minutes, then were baked at 165 degrees for 30 minutes. The devices were removed from a hot plate and cooled for 15 minutes. The Tygon ® tubing was inserted into the inlets, and the outlets of the device. Syringes were separately filled with the oil phases (perfluorodecalin with 1H, 1H, 2H, 2H-perfluoro-1-octanol surfactant and hydrofluoroether with RAN 008-Fluoro-Surfactant), and the aqueous phases: PBS, and ferricyanide dissolved in PBS. Needles were then threaded onto the syringes, the syringes were placed inside the syringe pumps, and the flow of the oil phase and aqueous phase was controlled by the syringe pump.

2.5 Electrochemical Characterization and Analysis

Carbon paste electrodes were cleaned by rinsing with 70% ethanol, followed by rinsing with distilled H20 and were then air dried. To check for electrode fouling prior to measurements, a blank measurement using PBS was performed. If no peaks were visible in the PBS blank measurement, the devices were clean and ready for use. For bulk scale DPV measurements using the glassy

carbon working electrode, the modulation amplitude was 200 mV with a step potential of 200 mV and a scan rate of 100 mV•$s^{-1.}$ For bulk scale CV measurements using the glassy carbon working electrode, the step potential was 10 mV and the scan rate was 100 mV•s^{-1}. For DPV measurements using the Cr-CPE electrode, the modulation amplitude was 40 mV with a step potential of 10 mV and a scan rate of 20 mV• s^{-1}. For CV measurements using the Cr-CPE electrode, the step potential was 7 mV and the scan rate was 100 mV• s^{-1}. For measurements using the Cr-CPE sensor, 18 µL of solution containing the analytical standard, yeast, or both were pipetted onto the sensor surface. Between each measurement, 18 µL of PBS was pipetted onto the sensor surface. For droplet detection, aqueous droplets containing 1 mM ferricyanide were generated at the T-junction using an oil carrier phase, consisting of perfluorodecalin and 1H, 1H, 2H, 2H-perfluoro-1-octanol as a surfactant at a ratio of 10:2 v/v respectively, or hydrofluoroether and RAN 008-Fluoro-Surfactant at a ratio of 0.5 % v/v.. Flow rates of the aqueous and oil phase were modulated using New Era 1000-US syringe pumps (Suffolk County, NY, USA). The flow rates used for droplet generation were 70 µL/min for the oil phase, and 10 µL/min for the aqueous flow. Droplets generated on the device were 1000 µm diameter, 100 µm height, with ~300 nL volume. Applied potentials for chronoamperometry experiments were -0.5 V for potassium ferricyanide measurements, and 0.25 V for (S)-reticuline measurements.

2.6 Yeast culture

S. cerevisiae yeast strains BY4741 and LN1069 were cultured following the previously described microtiter plate assay protocol for measuring yeast produced BIA's[23]. Primarily, glycerol stocks were streaked out on yeast extract peptone dextrose (YPD) plates. Colonies were picked in

triplicates and cultured in 500 µL of 2× SCS medium (13.4 g•L^{-1} BD Difco Yeast Nitrogen Base without amino acids, 2× drop-out Medium Supplements minus appropriate amino acids, 40 g•L^{-1} sucrose) within 96-well deep well plates at 30 °C. Following 16–24 h of growth, saturated cultures were diluted 50-fold into 0.5 mL of fresh 2× SCS medium in 96-well deep well plates. Cultures were grown at 30 °C with shaking at 2000 rpm. Following 72–96 h of growth, OD_{600} measurements were taken using a TECAN Infinite M200 well plate reader measuring at 600 nm, in the GE 300 room of the Concordia CASB building using 25 flashes, and the yeast culture was diluted in PBS to obtain a final OD_{600} of 0.079, 0.980, 5.890 and 9.120.

2.7 Graphical analysis and data processing

Electrochemical data processing was done using PSTrace 5.9. For cyclic voltammetry, high smoothing was applied. For differential pulse voltammetry, high smoothing, and non-linear baseline adjustment were applied. For chronoamperometry, non-linear baseline adjustment was applied. Student's t-test was used to evaluate the significance of difference between mean current responses from test samples and control samples, including droplets containing potassium ferricyanide and those not containing potassium ferricyanide, and differences in peak current after coating electrodes with fluorinated oils. Peak current and voltage were calculated using PSTrace 5.9. Standard curves were evaluated based on R^2 value. Measurements were performed in triplicates. Statistical analysis was carried out in GraphPad Prism 8. ANOVA was used to evaluate differences in peak potential (E_p) of BIA biosynthesis intermediates.

2.8 LC/MS analysis

Analytical standard of (*S*)-reticuline was diluted in 0.1% formic acid in mass spectrometry grade water to a final concentration of 0.1, 1 and 5 µM to a final volume of 1 mL. Samples were prepared for LC/MS by extracting (*S*)-reticuline from cell culture supernatant. Yeast cells were pelleted by centrifugation at 21,130 RCF for 5 minutes. 20 µL of supernatant dissolved into 80 µL of acetonitrile in a 1.5 mL centrifuge tube. The samples were incubated for 10 minutes at room temperature. The samples were centrifuged at 13000 rpm for 5 minutes. 50 µL of supernatant was moved to a fresh centrifuge tube; and added to 950 µL 0.1% formic acid in mass spectrometry grade water. LC/MS analysis was performed using Agilent LC/MS-QTOF.

Chapter 3 Results and Discussion

Here we present results showing a proof of concept for automated high throughput screening of a yeast library that produces (S)-reticuline. First, we show that (S)-reticuline can be detected using electrochemical analysis. Then, we showcase a device which is fabricated using a method that solves mechanical problems with traditional carbon paste electrodes that are integrated with microfluidics. This lab on a chip technology can selectively measure (S)-reticuline in the presence of BIA precursors, can sense (S)-reticuline in the presence of yeast culture and can detect droplet contents. To the best of our knowledge, this is the first study using electrochemistry to measure metabolites produced through a heterologous biosynthesis pathway.

3.1 Bulk scale electrochemical detection of (*S*)-reticuline

Glassy carbon electrodes have been used to detect precursors in the yeast biosynthesis pathway which produces (*S*)-reticuline[106–108]. To evaluate success is by determining whether there is improved peak separation between the peak for oxidation and reduction, and it is known that the (*S*)-reticuline precursor dopamine oxidizes and reduces on a carbon electrode[85]. In initial experiments, we show detection of (*S*)-reticuline, and the peak separation between (*S*)-reticuline and dopamine using a glassy carbon working electrode in a bulk scale electrochemical cell. As shown in **Figure 3-1A**, are two cyclic voltammograms of a blank sample containing only PBS and a sample containing 9 μM of (*S*)-reticuline in PBS. Using the glassy carbon resulted in an oxidation peak at 430 mV and a reduction peak at 219 mV (peak height ratio of 0.49) and a peak potential separation of 211 mV. These peaks and separation are not observed for the blank

measurement in the same current range of -0.4 to +0.4 μA (**Figure 3-1B**).

In addition, we performed DPV measurements for different concentrations of (*S*)-reticuline and compared their oxidation/reduction peak potential separation difference with dopamine. This concentration range was chosen, because later experiments showed that yeast diluted into PBS to a concentration at which (*S*)-reticuline oxidation peaks were visible, is a dilution factor at which we expect to see approximately this concentration of (*S*)-reticuline (**Figure 3-4D**). The difference between the peak reduction potential of dopamine (**Figure 3-1C**) and (*S*)-reticuline (**Figure 3-1D**) was ~51 mV, while the difference between the peak oxidation potentials of dopamine (**Figure 3-1E)** and (*S*)-reticuline (**Figure 3-1F)** was 252 mV. Since oxidation of dopamine and (*S*)-reticuline showed a greater difference in peak potential than reduction, there is higher selectivity for detecting (*S*)-reticuline in the presence of dopamine by oxidation than by reduction using a glassy carbon electrode. Furthermore, using oxidation (and reduction), we can detect peak current differences for (*S*)-reticuline. At lower concentration of (*S*)-reticuline, we observe a broad peak at 381 mV, which separate to two peaks at higher concentrations, with the second peak visible at 480 mV. The first peak is due to the oxidation of (*S*)-reticuline to (*S*)-scoulerine, while the second peak is expected due to the oxidation of (*S*)-scoulerine to dehydroscoulerine[109]. Regardless, detection of (*S*)-reticuline using a glassy carbon electrode is a suitable system for electrochemical (*S*)-reticuline detection. Improved peak separation using oxidation between (*S*)-reticuline and the precursor dopamine allows us to more selectively detect (*S*)-reticuline, which is necessary for the measurement of (*S*)-reticuline in yeast culture, which contains precursors in the biosynthesis pathway, including dopamine.

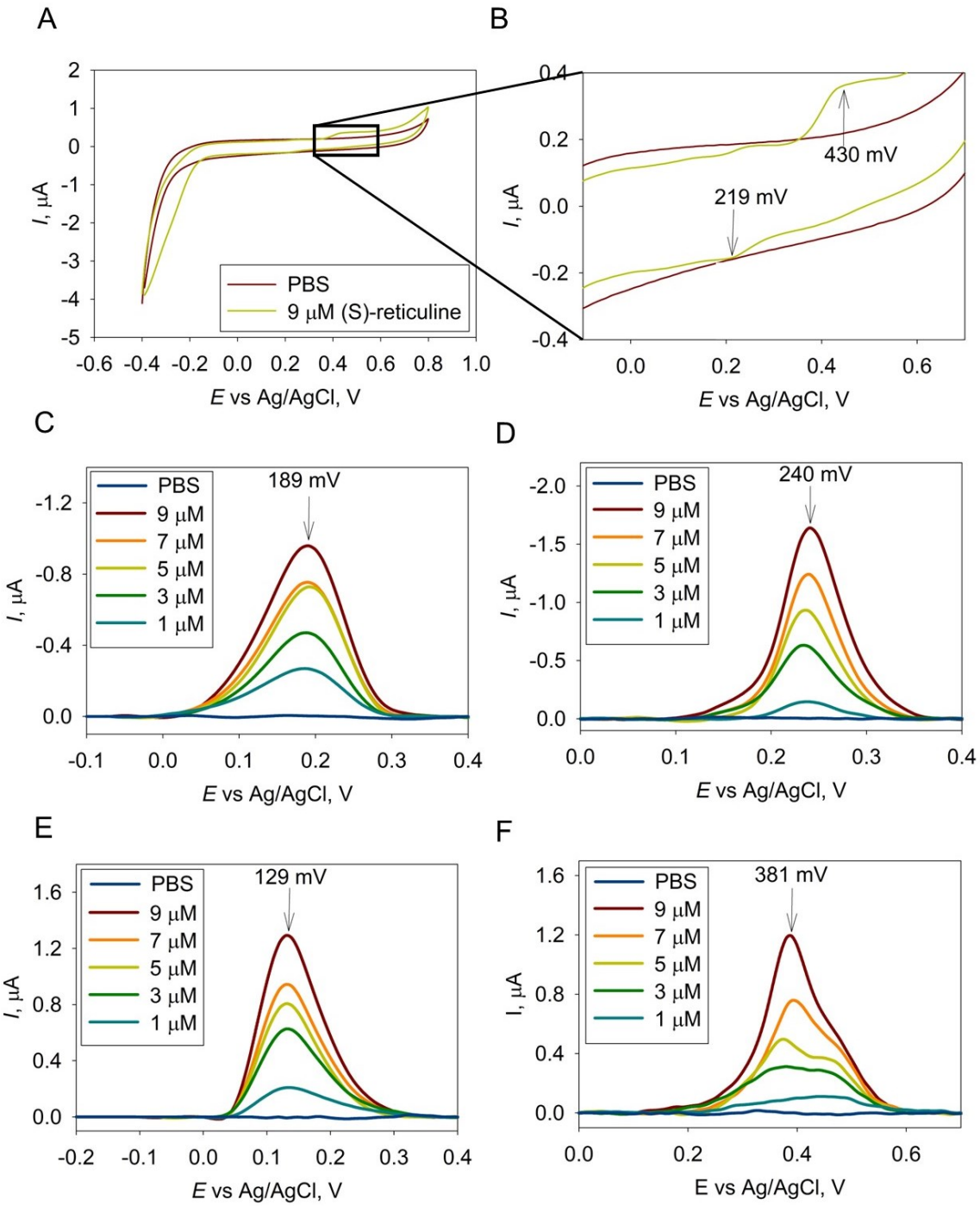

Figure 3-1 Electrochemical detection of (*S*)-reticuline using a glassy working carbon electrode for different concentrations of (*S*)-reticuline and dopamine.

(A) CV of (S)-reticuline vs PBS blank, (B) A zoomed-in view showing (with arrows) the oxidation and reduction peaks of (*S*)-reticuline. (C) Reduction DPV of dopamine and (D) (*S*)-reticuline. (E) Oxidation DPV of dopamine and (F) (*S*)-reticuline. All arrows with labeled potentials represent the peak potential.

3.2 Chromium-carbon paste sensor for selective detection of (*S*)-reticuline

Carbon-paste electrodes are extremely attractive for electrochemical sensing due to their cheap costs, ease of fabrication, and there have been many derivatives of these types of electrodes integrated in microfluidic devices[80,81,92,97,110,111]. Here, we add to these works and developed a sensor fabricated with chromium wires connected with carbon paste reference, counter and working electrodes that is shown to have improved mechanical stability compared to only using carbon paste electrodes that are screen printed into PDMS channels. Mechanical stability of micro-electrodes is a problem. Smaller electrodes are at greater risk of mechanical, thermal and chemically induced damage[112,113]. The current solution to this problem is to repair the electrodes by bridging the gaps (cracks) using carbon nanotubes[104], which is tedious and time consuming. In initial device fabrication procedures, screen printing carbon paste PDMS electrodes in PDMS channels requires support pillars to keep the carbon paste inside the channel during removal of the excess carbon paste (**Figure 3-2A**). In addition, fabricating these electrodes in PDMS channels generates cracks in the carbon paste wires, as shown by SEM imaging (**Figure 3-2B)**. PDMS is a relatively flexible material (Young's modulus of 1.32-2.97 MPa[114]) and the carbon paste electrodes within PDMS channels, causes the carbon paste to break. Instead, we created channels using SU-8, a more rigid material (Young's modulus 3.8-5.4 GPa[115]) and patterning the SU-8 above a chromium wire layer to create apertures in the SU-8 which we filled with carbon paste, creating carbon paste electrodes with chromium connections (which we call "Cr-CPE"). The Cr-CPE electrodes connect through the chromium wires to a potentiostat (**Figure 3-2C**). SEM imaging of the Cr-CPE showed minimal or completely absence of cracks, and the fabrication method did not

require pillars to keep the carbon paste inside the channel during removal of the excess carbon paste (**Figure 3-2D**). By removing PDMS pillars, the surface area of the electrodes and their electrochemical measurement sensitivity are greatly improved given that surface area is proportional to peak current (Equation 1-2).

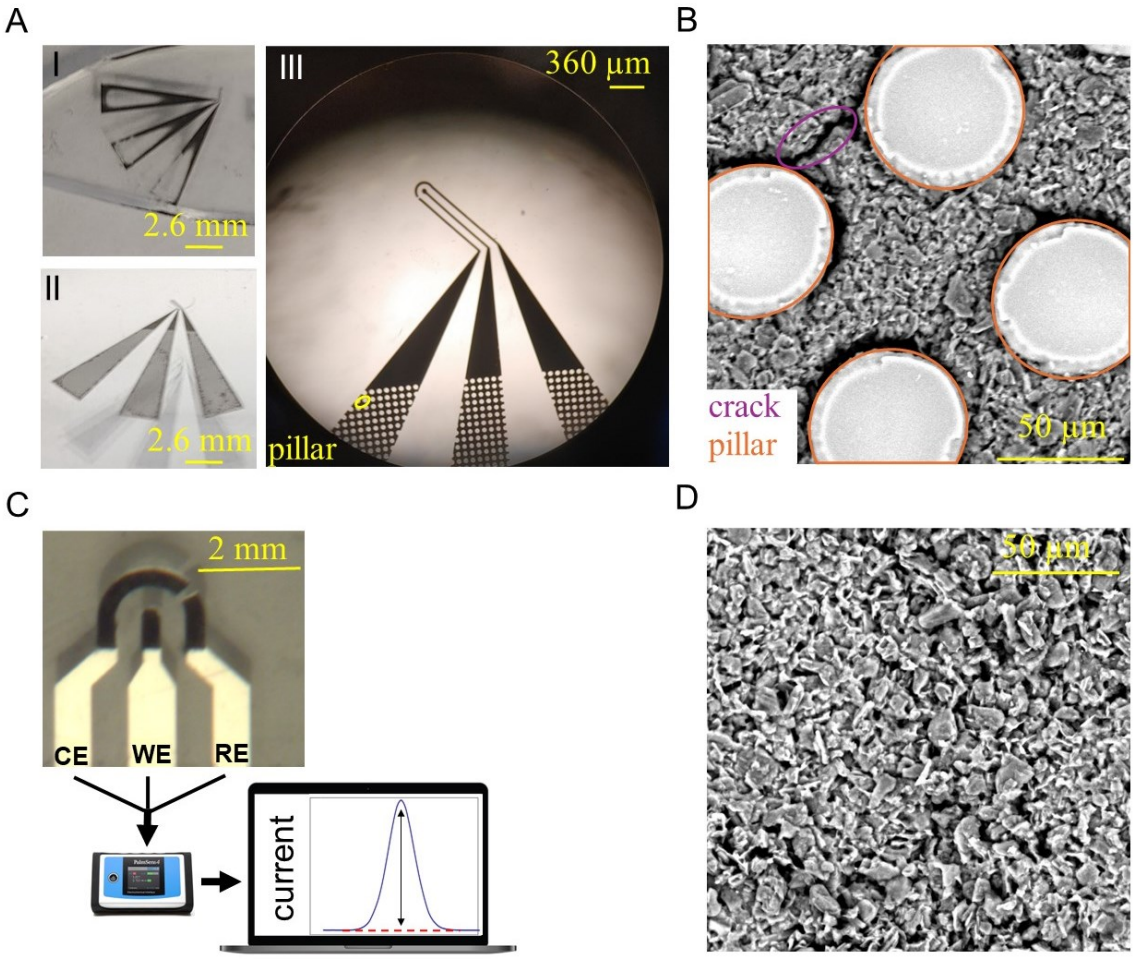

Figure 3-2 A chromium-carbon paste electrochemical sensor

Carbon paste electrodes in PDMS without support pillars (A-I), carbon paste electrodes in PDMS with support pillars (A-II, 10x magnification: A-III). SEM imaging of carbon paste electrodes with support pillars (B). Cr-CPE allows a connection to be formed using chromium wires, which connect to a potentiostat (C). SEM of Cr-CPE electrodes showed no cracks (D).

To demonstrate that the Cr-CPE sensor has reliable connections, and that it can be used to selectively detect (*S*)-reticuline, we performed a series of electrochemical measurements and compared it to all-gold electrochemical cell measurements. First, we evaluated our device with a CV measurement of a redox indicator (potassium ferricyanide). Potassium ferrocyanide was chosen as a model analyte, as it is commonly used for characterizing electrochemical oxidation and reduction reactions[116–118]. The useful potential window, for 1 mM potassium ferrocyanide, is at approximately -0.8 V, to +0.8 V, to observe both oxidation and reduction reactions. At 0.0975 V, we observe an oxidation peak, and at -0.542 V we observe a reduction peak. These oxidation and reduction peaks, as shown in **Figure 3-3A,** show a peak height ratio of 2.26 and a peak separation of 639 mV. Our system is expected, comparing to Randles-Sevcik equation (Equation 1-2), to produce a voltammogram with reduction and oxidation peaks of equal height, separated by ~59 mV at room temperature if it is a reversible electrochemical system: a system in which there is a low barrier to electron transfer between the electrode and the analyte[77]. Screen printed carbon electrodes have little to no reversibility[119], which explains the difference in peak current between our oxidation and reduction current peaks, as well as the peak potential separation greater than ~59 mV, when measuring ferricyanide, which shows reversible behaviour using cyclic voltammetry using different material as the working electrode[120]. This low reversibility is attributed to the poor charge transfer due to highly resistive electrode components[121]. The carbon paste used to fabricate the Cr-CPE is 50 % w/w PDMS, and PDMS is typically used as an insulator[114], which explains the high resistance in the Cr-CPE. However, the level of precision observed for multiple measurements using different devices, provided a low standard deviation of 0.6 and 2.2 % for the peak height of oxidation and reduction respectively.

Next, we tested standards of the metabolite, (*S*)-reticuline, for both all-gold standard and our Cr-CPE devices. All-gold electrodes have been integrated with microfluidic devices for electrochemical measurements[122]. In our work, we found that at high concentrations of (*S*)-reticuline (200 μM), there was a minimal difference in peak current via oxidation at 0 V compared to a blank (**Figure 3-3B**). As shown in **Figure 3-3C**, we were able to detect (*S*)-reticuline in a much lower (2-10 μM) concentration range, with an LOD of 0.5 μM using the Cr-CPE. Since clear oxidation peaks were observed in the 2-10 μM concentration range for detecting (*S*)-reticuline produced by the yeast, and this was confirmed with LC/MS (**Figure 3-4D**) we proceeded with the Cr-CPE electrodes. In addition, we observe less than 10 mV of potential drift between different scans and concentrations, and this level of potential drift is suitable for electrochemical measurements in droplets[123]. As shown in **Figure 3-3D**, there is an excellent linear relationship between oxidation peak current and concentration of (*S*)-reticuline in the μM concentration range (R^2 = 0.9443), which indicates that our sensor is sensitive at the desired concentrations of (*S*)-reticuline. We additionally performed cross-reactivity experiments with other interesting (and similar chemical structure) metabolites as (*S*)-reticuline. L-DOPA, dopamine and (*S*)-norcauclaurine are precursors to (*S*)-reticuline in the biosynthesis pathway in yeast (**Figure 1-3**). From **Figure 3-3E,** there are large peak shifts (at least 150 mV) between the metabolites. Plotting the peak current for (*S*)-reticuline compared to dopamine, L-DOPA and (*S*)-norcauclaurine shows a significant difference (P = 0.0015, N = 3 **Figure 3-3F**), demonstrating that this sensor can selectively detect (*S*)-reticuline in the presence of precursors in the metabolic pathway that produces (*S*)-reticuline in yeast. The differences in peak potential between (*S*)-reticuline and the other metabolites suggest that our sensor is suitable for droplet detection.

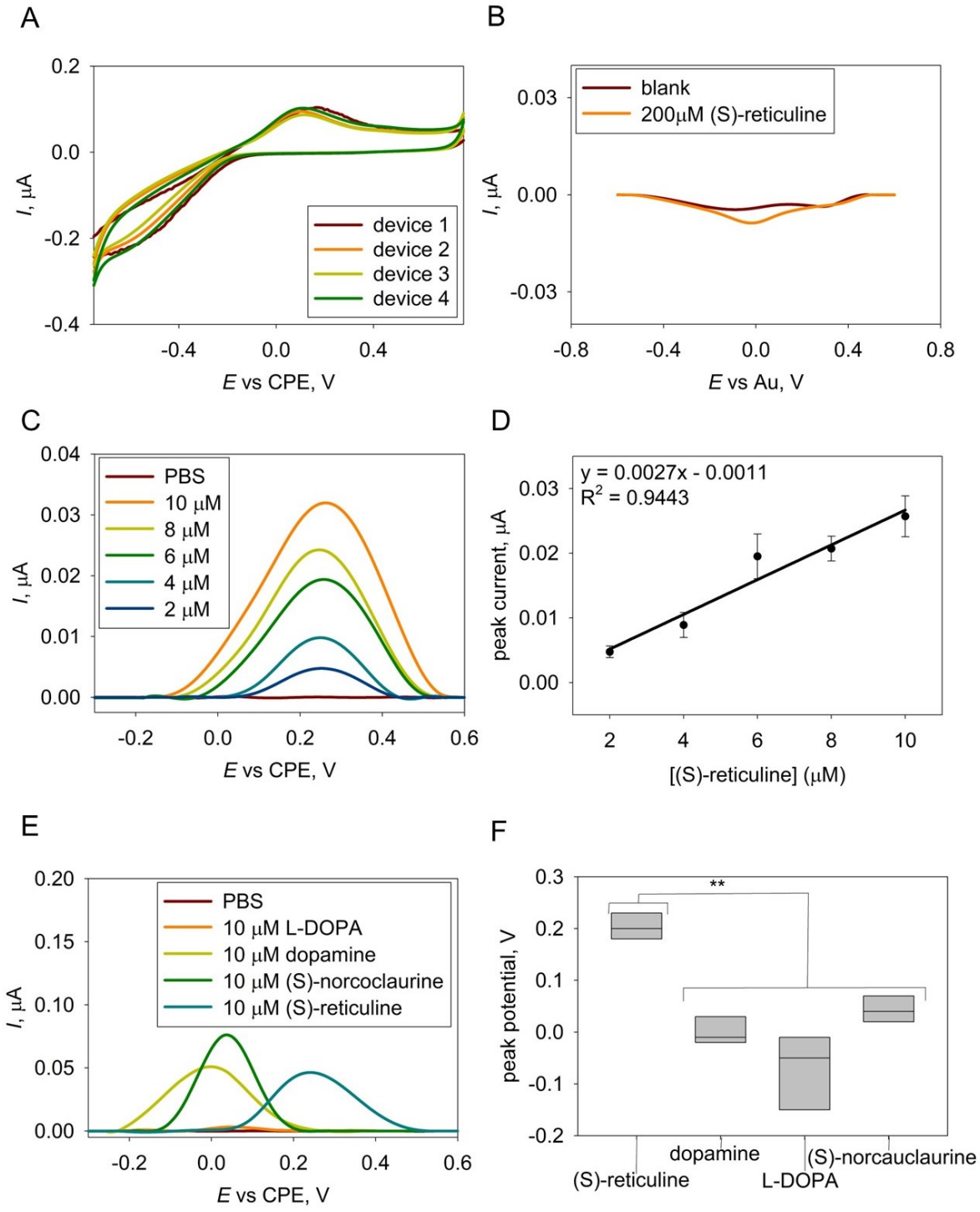

Figure 3-3 Detection of (*S*)-reticuline at a chromium-carbon paste electrochemical sensor by drop-casting.

(A) Reproducibility of Cyclic Voltammetry of 1mM potassium ferricyanide in PBS at 4 Cr-CPE devices at 100 mV/s. Differential pulse voltammetry analysis of (*S*)-reticuline for (B) all-gold and (C) Cr-CPE device. For (B), only one concentration was performed due to the minimal peak ratio between the sample and blank at very high concentration of (*S*)-reticuline (200 µM). For (C), the peak current were obtained from different

(S)-reticuline concentrations to plot (D) a standard curve in the 2-10 μM range. Differential pulse voltammetry of dopamine, L-DOPA, (*S*)-norcauclaurine and (*S*)-reticuline (E). Differences in oxidation peak potential of (*S*)-reticuline compared to precursors L-DOPA, dopamine and (*S*)-norcauclaurine showing a significant difference in peak oxidation potential between (*S*)-reticuline and the precursors dopamine, L-DOPA, (*S*)-norcauclaurine (**P=0.0015) (F). The line shown in the bars describe the mean peak potential. For experiments showing replicates, three independent replicates were performed.

3.3 Detection of (S)-reticuline produced by engineered yeast

The new Cr-CPE electrochemical sensor was applied to detecting (*S*)-reticuline produced by engineered yeast, motivated by the need to find rapid techniques to detect non-fluorescent metabolites[124]. Previous reports have shown that cell culture medium affects electrochemical measurements[125,126]. *S. cerevisiae* yeast is predict to potentially secrete 156 proteins[127], and proteins are known to adsorb and accumulate (or "foul") on the electrode surface. Such fouling generates an impermeable membrane on the surface, which prevents contact between the analyte and the electrode[128]. Between 10-100 μM, we were able to detect (*S*)-reticuline in pure YPD culture media using a glassy carbon electrode, however there was ~3x lower peak current using YPD as the supporting electrolyte to detect 10 μM (*S*)-reticuline compared to 9 μM (*S*)-reticuline in PBS (**Figure S-1, Figure 3-1D**). While the standard culture media for yeast may not be suitable for electrochemical detection, there is a study that has demonstrated that yeast can temporarily survive while suspended in PBS[129].

PBS is a preferred electrochemical solution due to its high conductivity resulting from high salt content, making it commonly used as a solvent in electrochemical experiments for droplet microfluidics[82]. We performed DPV measurements of (*S*)-reticuline producing yeast at various dilution factors with PBS ranging from no dilution (100 % yeast culture) to yeast cultured in SCS diluted 100-fold in PBS (1% yeast culture). As shown in **Figure 3-4A,** as expected, with pure yeast

culture and with culture diluted to 65%, we observed close to 0 μA current. It is not until, the dilution factor of 10-fold (10% yeast culture) with PBS that we observe two current peaks, and we see that these two peaks are shifted towards more positive potentials in the 10% yeast culture compared to the 1% yeast culture. The shift towards positive potentials is most likely due to the reference electrode being fouled. 1% yeast culture also showed the highest peak current (**Figure 3-4B**) therefore 1% yeast culture was chosen as the optimal dilution ratio for further experiments.

Next, we investigated whether these peaks were caused by the oxidation of other metabolites produced by yeast, that are not part of the BIA biosynthesis pathway. We observed one oxidation peak at the potential of 139 mV, which is close to the peak oxidation potential observed for the (*S*)-reticuline precursors L-DOPA, dopamine, and (*S*)-norcauclaurine. We observed a second oxidation peak at 349 mV, which is close to the oxidation potential of (*S*)-reticuline at the Cr-CPE electrode. These two peaks were not present in the yeast wild-type strain, which does not produce (*S*)-reticuline diluted the same amount (**Figure 3-4C**).

Two factors explain the presence of (*S*)-reticuline oxidation peaks at lower concentrations diluted into PBS but not at higher concentrations: concentration of fouling agents from the yeast media, and the concentration of the supporting electrolyte (PBS). The higher cell density samples contain more fouling agents, which reduce the bare electrode surface area and inevitably reduces the signal current. The higher cell density samples also have less electrolytes from PBS, and electrolytes are necessary for electrochemical measurements. Of the two cell densities that do show (*S*)-reticuline oxidation peaks, the higher cell density is shifted towards a more positive potential, and it has been shown that fouling of the reference electrode shifts potential in a positive direction[130] (**Figure 3-4D**). Overall, these findings show that we can detect (*S*)-reticuline on the device, and that diluting the yeast into PBS 100 fold is optimal for electrochemical measusrements.

Diluting the yeast culture in PBS allows us to measure (*S*)-reticuline in the droplets, and recover the yeast cells after the measurement.

To validate the Cr-CPE electrode as an analytical tool, we verified the measurements with LC/MS, and observed that at the 100-fold dilution, the yeast strain was producing ~7 µM (*S*)-reticuline. We interpolated the yeast (*S*)-reticuline production from the standard curve of our device (**Figure 3-3C**), and saw that according to that standard curve, the yeast at that dilution should be producing 5 µM (*S*)-reticuline, showing a 29% difference in measurement between the device and LC/MS (**Figure 3-4D**) We hypothesize that the lesser amount of (*S*)-reticuline measured on the device compared to LC/MS is due to electrode fouling from proteins in the yeast media, which are not present in the measurements used for the standard curve.

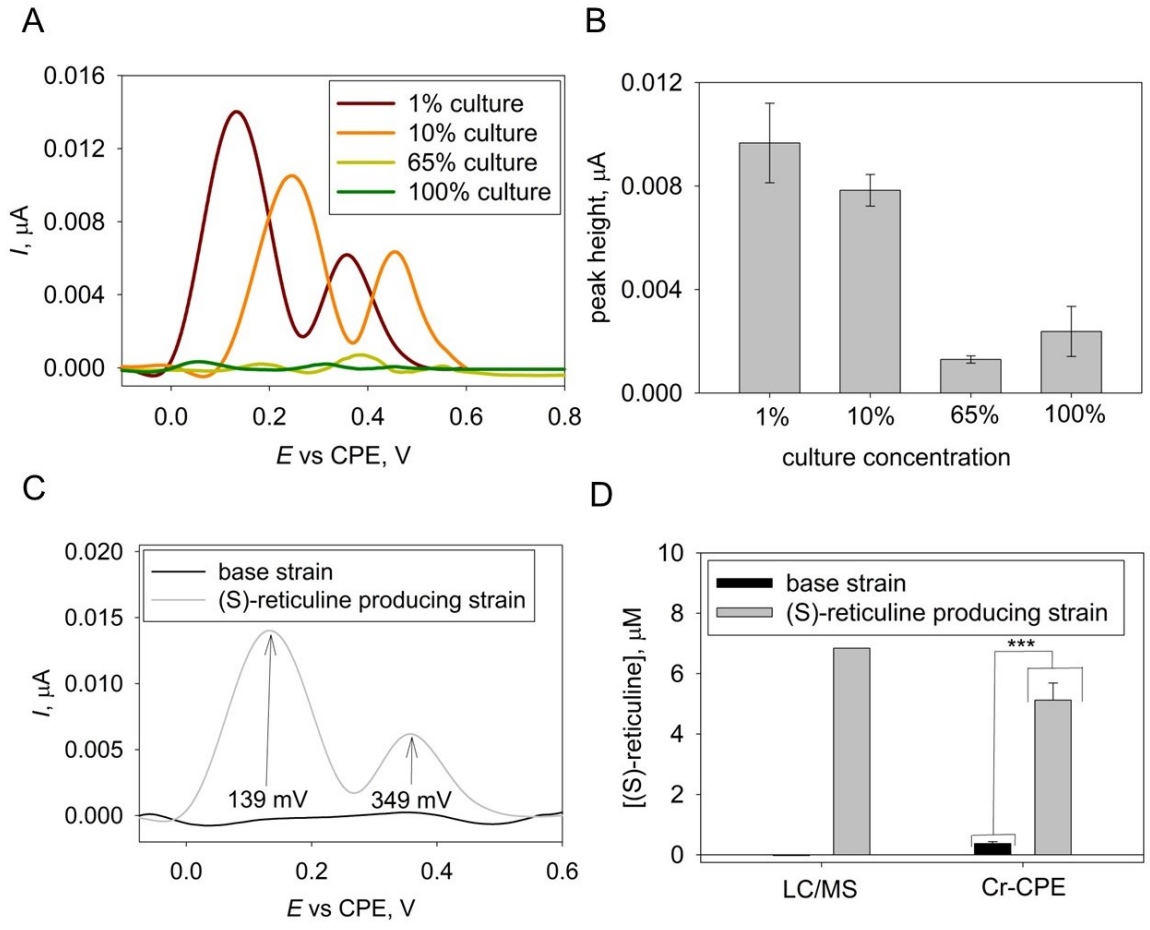

Figure 3-4 Detection of (*S*)-reticuline produced by yeast

DPV (A) and peak current height (B) of (*S*)-reticuline producing yeast diluted in PBS at different ratios of yeast culture to PBS. In (A) and (B), percentage listed is the percentage of the measured solution which was yeast culture, while the rest of the solution is made up of PBS. Oxidation DPVs of (*S*)-reticuline producing yeast vs a yeast strain that does not produce (*S*)-reticuline (C). LC/MS validation of the Cr-CPE device for measurement of yeast produced (*S*)-reticuline after 100 fold dilution into PBS (D). OD600 of the (*S*)-reticuline producing strain and base strain were 9.11 and 10.1 respectively.

3.4 Integrating Cr-CPE with droplet microfluidics

Droplet sorting using electrodes is available in the literature[49,131–133], however, in terms of using them as the detection method for sorting is relatively rare. The reason is the sample that is being detected must reside on the electrodes for a long enough time to scan a range of potentials or being able to obtain a signal from the analyte, which can be challenging when the throughput rates are pushing towards the kHz range[70,133]. One electrochemical method to use for detecting droplets at a rapid rate is chronoamperometry. Chronoamperometry (CA) applies a fixed potential, and measures current over time, and is the most common electroanalysis technique used in droplet microfluidics [82,96,97,123]. An additional challenge is the oil phase that contains surfactant (the carrier phase in droplet systems) since lipids are known to cause electrode fouling which can create irreproducibility in the measurements[128]. The purpose of this section is to demonstrate the Cr-CPE device can be used to detect droplet contents, and to identify an oil phase that can be used for generating droplets, and measuring (*S*)-reticuline in the relevant concentration range. Lipids are known to cause electrode fouling[128], however is necessary to generate droplets. For this reason, we investigated the use of fluorinated oils, to identify an oil that could be used as the oil phase which intersperses droplets to detect (*S*)-reticuline. We designed a droplet generating device, with a channel constriction, which elongates droplets, allowing larger surface area of contact between

the electrodes and the droplet to test the fluorinated oils as well as to perform CA measurements (**Figure 3-5A**).

As shown in **Figure 3-5B**, CA of droplets on the Cr-CPE device showed that there was a difference in oxidation peak height between droplets containing the redox indicator potassium ferricyanide and the solvent blank when using with perfluorodecalin oil with 20% perfluorooctanol surfactant as an oil phase (**Figure 3-5B**). On average on scanning 16 droplets, we observe an average peak height of 0.03 μA for the sample and close to minimal peak current (0.004 μA) for the blank (**Figure -5C**). This increase in peak height in droplets containing analyte compared to empty droplets is in line with previous reports measuring analytes in the millimolar range using this oil phase[82,97]. The detection of potassium ferricyanide demonstrates that this device can be used to measure the constituents inside the droplet. To mimic the interface between the electrode sensor and the droplet in a droplet microfluidic device, we coated the surface of the sensor with fluorinated oil. Droplets are interspersed with fluorinated oil, and a layer of oil may be present between the droplet and the electrodes when measuring droplet contents. (*S*)-reticuline showed no difference in current response compared to a solvent blank after coating the surface of the electrode with perfluorodecalin oil with 20% perfluorooctanol surfactant (**Figure 3-5D**). After coating the sensor with a different oil phase: hydrofluoroether (HFE) oil with 0.5% RAN surfactant, there was a difference in current response (**Figure 3-5E**). Since we can detect (*S*)-reticuline after coating the electrode with hydrofluoroether (HFE) oil with 0.5% RAN surfactant, this oil phase is ideal for droplet measurement experiments of (*S*)-reticuline.

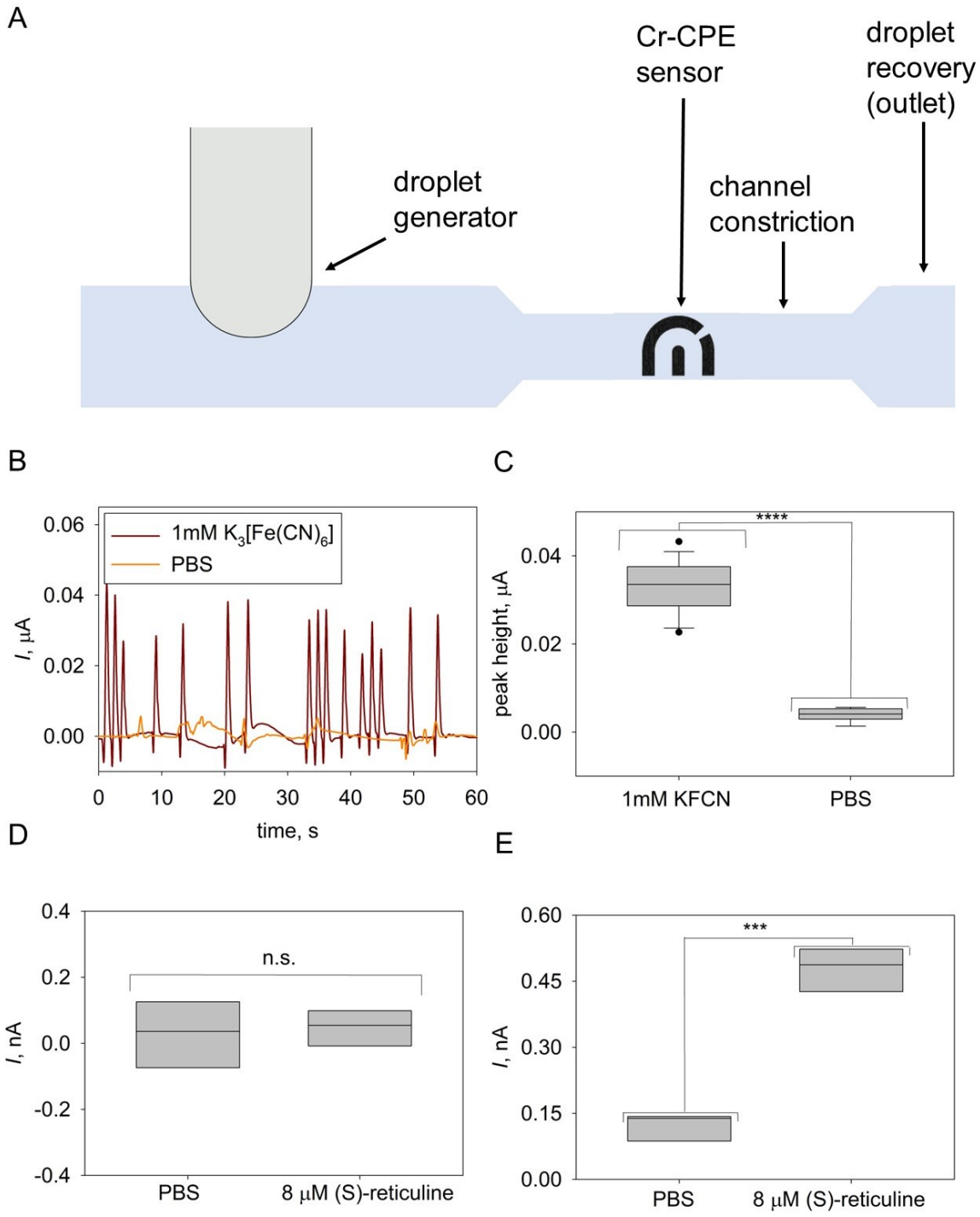

Figure 3-5 Detection of droplet contents using Cr-CPE

Droplets are generated at a droplet generator, pass through a channel constriction, which elongates the droplets, allowing simultaneous exposure of the droplet contents to the sensing electrodes, and an outlet is used to recover the droplets (A). Chronoamperometry of droplets containing 1mM potassium ferricyanide ($K_3[Fe(CN)_6]$) vs droplets containing solvent (PBS) on the Cr-CPE device (B). Distribution of peak height of droplets containing 1 mM potassium ferricyanide vs PBS (C). Oxidation current of (*S*)-reticuline after

flow injection of perfluorodecalin oil with 20% perfluorooctanol surfactant (D). Oxidation current of (S)-reticuline after flow injection of hydrofluoroether (HFE) oil with 0.5% RAN surfactant (E).

Chapter 4 Concluding Remarks

4.1 Conclusion

We developed a novel electrochemical sensor that solves the problem of mechanical instability of previous carbon paste electrochemical sensors that are integrated with microfluidics. We demonstrated that using this sensor, we could detect (*S*)-reticuline with a linear current response, demonstrating it has analytical value. We determined that this sensor is selective for detecting (*S*)-reticuline in the presence of other BIA's in the (*S*)-reticuline biosynthesis pathway. We used this device to detect (*S*)-reticuline in fermented yeast growth medium, and validated the results using LC/MS. We showed that this device can be used for detecting droplet contents.

4.2 Future outlook

An electrochemical sensor that is fabricated using a glass substrate, a chromium wire layer, and an SU8 layer allows future work to integrate this sensor with a coplanar droplet sorter[21] on a single chip, since the coplanar sorter, and the sensor can be fabricated by patterning chromium electrodes on a glass substrate, followed by patterning SU-8 above the chromium layer. Having encapsulation of yeast in droplets, as well as electrochemical droplet measurement and sorting on a single microfluidic device will allow sorting of libraries of droplet containing reticuline producing yeast.

Screening a library of (*S*)-reticuline producing cells is useful for improvement of (*S*)-reticuline yield. Further, screening yeast expressing new enzyme variants on this device may also

produce a suite of new to nature molecules in the BIA class, as well as others. Most importantly, this workflow for yield improvement can be used for other bioprocess improvement applications. In theory, any electroactive molecule that is produced using metabolically engineered yeast and secreted into surrounding medium could be detected using this device, if it has appropriate selectivity in the selected biological context.

High throughput analysis is critical in the broader scope of the design, build test learn cycle (**Figure 1-1**) of metabolic engineering. Since there are high throughput tools for the generation of engineered yeast strains[134] which automate the build step of the metabolic engineering cycle, and novel data analysis tools for learning from massive biological data sets[135], high throughput analysis tools bring us closer to automating the entire metabolic engineering workflow using high throughput tools. With high throughput tools for each step in the metabolic engineering workflow, the entire process can be performed in parallel rather than in series, which will accelerate the entire strain development process.

References

1. Dashko, S., Zhou, N., Compagno, C. & Piškur, J. Why, when, and how did yeast evolve alcoholic fermentation? *FEMS Yeast Res.* **14**, 826–832 (2014).
2. Wisselink, H. W., Toirkens, M. J., Wu, Q., Pronk, J. T. & van Maris, A. J. A. Novel Evolutionary Engineering Approach for Accelerated Utilization of Glucose, Xylose, and Arabinose Mixtures by Engineered Saccharomyces cerevisiae Strains. *Appl. Environ. Microbiol.* **75**, 907–914 (2009).
3. Zhang, Y.-X. *et al.* Genome shuffling leads to rapid phenotypic improvement in bacteria. *Nature* **415**, 644–646 (2002).
4. Stephanopoulos, G., Aristidou, A. A. & Nielsen, J. *Metabolic Engineering: Principles and Methodologies*. (Elsevier, 1998).
5. Thak, E. J., Yoo, S. J., Moon, H. Y. & Kang, H. A. Yeast synthetic biology for designed cell factories producing secretory recombinant proteins. *FEMS Yeast Res.* **20**, foaa009 (2020).
6. Cho, J. S., Kim, G. B., Eun, H., Moon, C. W. & Lee, S. Y. Designing Microbial Cell Factories for the Production of Chemicals. *JACS Au* **2**, 1781–1799 (2022).
7. Zhang, J., Zhu, Y., Zhang, W. & Mu, W. Efficient Production of a Functional Human Milk Oligosaccharide 3′-Sialyllactose in Genetically Engineered Escherichia coli. *ACS Synth. Biol.* **11**, 2837–2845 (2022).
8. Luo, Z. W., Cho, J. S. & Lee, S. Y. Microbial production of methyl anthranilate, a grape flavor compound. *Proc. Natl. Acad. Sci.* **116**, 10749–10756 (2019).
9. Liew, F. E. *et al.* Carbon-negative production of acetone and isopropanol by gas fermentation at industrial pilot scale. *Nat. Biotechnol.* **40**, 335–344 (2022).

10. Nakamura, C. E. & Whited, G. M. Metabolic engineering for the microbial production of 1,3-propanediol. *Curr. Opin. Biotechnol.* **14**, 454–459 (2003).

11. Keefer, L. M., Piron, M. A. & De Meyts, P. Human insulin prepared by recombinant DNA techniques and native human insulin interact identically with insulin receptors. *Proc. Natl. Acad. Sci.* **78**, 1391–1395 (1981).

12. Han, X. *et al.* The biosynthesis of papaverine proceeds via (S)-reticuline. *Phytochemistry* **71**, 1305–1312 (2010).

13. Caputi, L. *et al.* Missing enzymes in the biosynthesis of the anticancer drug vinblastine in Madagascar periwinkle. *Science* **360**, 1235–1239 (2018).

14. Marsafari, M. *et al.* Biotechnological Production of Flavonoids: An Update on Plant Metabolic Engineering, Microbial Host Selection, and Genetically Encoded Biosensors. *Biotechnol. J.* **15**, 1900432 (2020).

15. Adams, B. L. The Next Generation of Synthetic Biology Chassis: Moving Synthetic Biology from the Laboratory to the Field. *ACS Synth. Biol.* **5**, 1328–1330 (2016).

16. Hazelwood, L. A., Daran, J.-M., van Maris, A. J. A., Pronk, J. T. & Dickinson, J. R. The Ehrlich Pathway for Fusel Alcohol Production: a Century of Research on Saccharomyces cerevisiae Metabolism. *Appl. Environ. Microbiol.* **74**, 2259–2266 (2008).

17. Jordá, T. & Puig, S. Regulation of Ergosterol Biosynthesis in Saccharomyces cerevisiae. *Genes* **11**, 795 (2020).

18. Averesch, N. J. H. & Krömer, J. O. Metabolic Engineering of the Shikimate Pathway for Production of Aromatics and Derived Compounds—Present and Future Strain Construction Strategies. *Front. Bioeng. Biotechnol.* **6**, 32 (2018).

19. Galanie, S., Thodey, K., Trenchard, I. J., Filsinger Interrante, M. & Smolke, C. D. Complete biosynthesis of opioids in yeast. *Science* **349**, 1095–1100 (2015).

20. Zhang, Y., Nielsen, J. & Liu, Z. Engineering yeast metabolism for production of terpenoids for use as perfume ingredients, pharmaceuticals and biofuels. *FEMS Yeast Res.* **17**, fox080 (2017).

21. Han, J., Wu, Y., Zhou, Y. & Li, S. Engineering Saccharomyces cerevisiae to produce plant benzylisoquinoline alkaloids. *aBIOTECH* **2**, 264–275 (2021).

22. Zhang, J. *et al.* A microbial supply chain for production of the anti-cancer drug vinblastine. *Nature* **609**, 341–347 (2022).

23. Pyne, M. E. *et al.* A yeast platform for high-level synthesis of tetrahydroisoquinoline alkaloids. *Nat. Commun.* **11**, 3337 (2020).

24. Dykstra, C. B., Pyne, M. E. & Martin, V. J. J. CRAPS: Chromosomal-Repair-Assisted Pathway Shuffling in Yeast. *ACS Synth. Biol.* **12**, 2578–2587 (2023).

25. DeLoache, W. C. *et al.* An enzyme-coupled biosensor enables (S)-reticuline production in yeast from glucose. *Nat. Chem. Biol.* **11**, 465–471 (2015).

26. Yu, X. *et al.* CRISPRi-microfluidics screening enables genome-scale target identification for high-titer protein production and secretion. *Metab. Eng.* **75**, 192–204 (2023).

27. Petzold, C., Chan, L. J., Nhan, M. & Adams, P. Analytics for metabolic engineering. *Front. Bioeng. Biotechnol.* **3**, (2015).

28. UNODC - Bulletin on Narcotics - 1953 Issue 3 - 006. *United Nations : Office on Drugs and Crime* //www.unodc.org/unodc/en/data-and-analysis/bulletin/bulletin_1953-01-01_3_page007.html.

29. Ringel, M. S., Scannell, J. W., Baedeker, M. & Schulze, U. Breaking Eroom's Law. *Nat. Rev. Drug Discov.* **19**, 833–834 (2020).

30. Luo, X. *et al.* Complete biosynthesis of cannabinoids and their unnatural analogues in yeast. *Nature* **567**, 123–126 (2019).

31. Milne, N. *et al.* Metabolic engineering of Saccharomyces cerevisiae for the de novo production of psilocybin and related tryptamine derivatives. *Metab. Eng.* **60**, 25–36 (2020).

32. Paddon, C. J. & Keasling, J. D. Semi-synthetic artemisinin: a model for the use of synthetic biology in pharmaceutical development. *Nat. Rev. Microbiol.* **12**, 355–367 (2014).

33. Baeshen, N. A. *et al.* Cell factories for insulin production. *Microb. Cell Factories* **13**, 141 (2014).

34. Kjeldsen, T. *et al.* Molecular engineering of insulin for recombinant expression in yeast. *Trends Biotechnol.* **0**, (2023).

35. Hawkins, K. M. & Smolke, C. D. Production of benzylisoquinoline alkaloids in Saccharomyces cerevisiae. *Nat. Chem. Biol.* **4**, 564 (2008).

36. Frankel, J. P., Lees, A. J., Kempster, P. A. & Stern, G. M. Subcutaneous apomorphine in the treatment of Parkinson's disease. *J. Neurol. Neurosurg. Psychiatry* **53**, 96–101 (1990).

37. Ehrenworth, A. M. & Peralta-Yahya, P. Accelerating the semisynthesis of alkaloid-based drugs through metabolic engineering. *Nat. Chem. Biol.* **13**, 249–258 (2017).

38. The Selection and Use of Essential Medicines (2015) - TRS 994. https://www.who.int/publications-detail-redirect/9789241209946.

39. Sato, F. Chapter Six - Improved Production of Plant Isoquinoline Alkaloids by Metabolic Engineering. in *Advances in Botanical Research* (ed. Giglioli-Guivarc'h, N.) vol. 68 163–181 (Academic Press, 2013).

40. Fumihiko Sato. Plant Alkaloid Engineering. in (Elsevier, Graduate School of Biostudies, Kyoto University, Kyoto, Japan; Graduate School of Science, Osaka Prefecture University, Sakai, Japan, 2019).

41. Weid, M., Ziegler, J. & Kutchan, T. The roles of latex and the vascular bundle in morphine biosynthesis in the opium poppy, Papaver somniferum. *Proc. Natl. Acad. Sci. U. S. A.* **101**, 13957–62 (2004).

42. Onoyovwe, A. *et al.* Morphine Biosynthesis in Opium Poppy Involves Two Cell Types: Sieve Elements and Laticifers[W][OPEN]. *Plant Cell* **25**, 4110–4122 (2013).

43. Minami, H. *et al.* Microbial production of plant benzylisoquinoline alkaloids. *Proc. Natl. Acad. Sci. U. S. A.* **105**, 7393–7398 (2008).

44. Ethanol explained - U.S. Energy Information Administration (EIA). https://www.eia.gov/energyexplained/biofuels/ethanol.php.

45. Trenchard, I. J., Siddiqui, M. S., Thodey, K. & Smolke, C. D. De novo production of the key branch point benzylisoquinoline alkaloid reticuline in yeast. *Metab. Eng.* **31**, 74–83 (2015).

46. Narcross, L. *et al.* Benzylisoquinoline alkaloid production in yeast via norlaudanosoline improves selectivity and yield. 2023.05.19.541502 Preprint at https://doi.org/10.1101/2023.05.19.541502 (2023).

47. Narcross, L., Fossati, E., Bourgeois, L., Dueber, J. E. & Martin, V. J. J. Microbial Factories for the Production of Benzylisoquinoline Alkaloids. *Trends Biotechnol.* **34**, 228–241 (2016).

48. Tecan launches the Safire² microplate reader - monochromator power for a new level of speed and versatility in detection. https://www.tecan.com/customer-news/tecan-

launches-the-safire-sup-2-sup-microplate-reader-monochromator-power-for-a-new-level-of-speed-and-versatility-in-detection-2314.

49. Samlali, K., Alves, C. L., Jezernik, M. & Shih, S. C. C. Droplet digital microfluidic system for screening filamentous fungi based on enzymatic activity. *Microsyst. Nanoeng.* **8**, 123 (2022).

50. Miller, J. H. Mutagenic specificity of ultraviolet light. *J. Mol. Biol.* **182**, 45–65 (1985).

51. Ding, Y., Choo, J. & deMello, A. J. From single-molecule detection to next-generation sequencing: microfluidic droplets for high-throughput nucleic acid analysis. *Microfluid. Nanofluidics* **21**, 58 (2017).

52. Shembekar, N., Chaipan, C., Utharala, R. & Merten, C. A. Droplet-based microfluidics in drug discovery, transcriptomics and high-throughput molecular genetics. *Lab. Chip* **16**, 1314–1331 (2016).

53. Mazutis, L. *et al.* Single-cell analysis and sorting using droplet-based microfluidics. *Nat. Protoc.* **8**, 870–891 (2013).

54. Teh, S.-Y., Lin, R., Hung, L.-H. & P. Lee, A. Droplet microfluidics. *Lab. Chip* **8**, 198–220 (2008).

55. Ahmadi, F., Samlali, K., Vo, P. Q. N. & Shih, S. C. C. An integrated droplet-digital microfluidic system for on-demand droplet creation, mixing, incubation, and sorting. *Lab. Chip* **19**, 524–535 (2019).

56. Baret, J.-C. Surfactants in droplet-based microfluidics. *Lab. Chip* **12**, 422–433 (2012).

57. Zeng, W., Xiang, D. & Fu, H. Prediction of Droplet Production Speed by Measuring the Droplet Spacing Fluctuations in a Flow-Focusing Microdroplet Generator. *Micromachines* **10**, 812 (2019).

58. Gu, H., Duits, M. & Mugele, F. Droplets Formation and Merging in Two-Phase Flow Microfluidics. *Int. J. Mol. Sci.* **12**, 2572–97 (2011).

59. Yin, H. & Marshall, D. Microfluidics for single cell analysis. *Curr. Opin. Biotechnol.* **23**, 110–119 (2012).

60. Weaver, W. M. *et al.* Advances in High-Throughput Single-Cell Microtechnologies. *Curr. Opin. Biotechnol.* **0**, 114–123 (2014).

61. Reece, A. *et al.* Microfluidic techniques for high throughput single cell analysis. *Curr. Opin. Biotechnol.* **40**, 90–96 (2016).

62. Yang, S.-M. *et al.* Highly accurate multiprotein detection on a digital ELISA platform. *Lab. Chip* **22**, 3015–3024 (2022).

63. Wang, B. L. *et al.* Microfluidic high-throughput culturing of single cells for selection based on extracellular metabolite production or consumption. *Nat. Biotechnol.* **32**, 473–478 (2014).

64. Hu, P., Zhang, W., Xin, H. & Deng, G. Single Cell Isolation and Analysis. *Front. Cell Dev. Biol.* **4**, 116 (2016).

65. Collins, D. J., Neild, A., deMello, A., Liu, A.-Q. & Ai, Y. The Poisson distribution and beyond: methods for microfluidic droplet production and single cell encapsulation. *Lab. Chip* **15**, 3439–3459 (2015).

66. Baret, J.-C. *et al.* Fluorescence-activated droplet sorting (FADS): efficient microfluidic cell sorting based on enzymatic activity. *Lab. Chip* **9**, 1850–1858 (2009).

67. Medcalf, E. J., Gantz, M., Kaminski, T. S. & Hollfelder, F. Ultra-High-Throughput Absorbance-Activated Droplet Sorting for Enzyme Screening at Kilohertz Frequencies. *Anal. Chem.* **95**, 4597–4604 (2023).

68. Goto, H. *et al.* Microfluidic screening system based on boron-doped diamond electrodes and dielectrophoretic sorting for directed evolution of NAD(P)-dependent oxidoreductases. *Lab. Chip* **20**, 852–861 (2020).

69. Abate, A. R., Hung, T., Mary, P., Agresti, J. J. & Weitz, D. A. High-throughput injection with microfluidics using picoinjectors. *Proc. Natl. Acad. Sci.* **107**, 19163–19166 (2010).

70. Sciambi, A. & Abate, A. R. Accurate microfluidic sorting of droplets at 30 kHz. *Lab. Chip* **15**, 47–51 (2014).

71. Agresti, J. J. *et al.* Ultrahigh-throughput screening in drop-based microfluidics for directed evolution. *Proc. Natl. Acad. Sci.* **107**, 4004–4009 (2010).

72. Schnettler, J. D., Klein, O. J., Kaminski, T. S., Colin, P.-Y. & Hollfelder, F. Ultrahigh-Throughput Directed Evolution of a Metal-Free α/β-Hydrolase with a Cys-His-Asp Triad into an Efficient Phosphotriesterase. *J. Am. Chem. Soc.* **145**, 1083–1096 (2023).

73. Pyne, M. E. *et al.* Chapter Nine - Reconstituting Plant Secondary Metabolism in Saccharomyces cerevisiae for Production of High-Value Benzylisoquinoline Alkaloids. in *Methods in Enzymology* (ed. O'Connor, S. E.) vol. 575 195–224 (Academic Press, 2016).

74. Li, Y. *et al.* Complete biosynthesis of noscapine and halogenated alkaloids in yeast. *Proc. Natl. Acad. Sci. U. S. A.* **115**, E3922–E3931 (2018).

75. Ahmad, M., Wolberg, A. & Kahwaji, C. I. Biochemistry, Electron Transport Chain. in *StatPearls* (StatPearls Publishing, Treasure Island (FL), 2023).

76. Schmidt-Rohr, K. How Batteries Store and Release Energy: Explaining Basic Electrochemistry. *J. Chem. Educ.* **95**, 1801–1810 (2018).

77. Elgrishi, N. *et al.* A Practical Beginner's Guide to Cyclic Voltammetry. *J. Chem. Educ.* **95**, 197–206 (2018).

78. Vafaiee, M., Vossoughi, M., Mohammadpour, R. & Sasanpour, P. Gold-Plated Electrode with High Scratch Strength for Electrophysiological Recordings. *Sci. Rep.* **9**, 2985 (2019).

79. Coustan, L., Shul, G. & Bélanger, D. Electrochemical behavior of platinum, gold and glassy carbon electrodes in water-in-salt electrolyte. *Electrochem. Commun.* **77**, 89–92 (2017).

80. Gross, E. M. *et al.* Micromolded Carbon Paste Microelectrodes for Electrogenerated Chemiluminescent Detection on Microfluidic Devices. *ChemElectroChem* **7**, 3244–3252 (2020).

81. Sameenoi, Y. *et al.* Poly(dimethylsiloxane) cross-linked carbon paste electrodes for microfluidic electrochemical sensing. *Analyst* **136**, 3177–3184 (2011).

82. Suea-Ngam, A., Rattanarat, P., Chailapakul, O. & Srisa-Art, M. Electrochemical droplet-based microfluidics using chip-based carbon paste electrodes for high-throughput analysis in pharmaceutical applications. *Anal. Chim. Acta* **883**, 45–54 (2015).

83. Grieshaber, D., MacKenzie, R., Vörös, J. & Reimhult, E. Electrochemical Biosensors - Sensor Principles and Architectures. *Sensors* **8**, 1400–1458 (2008).

84. Martínez-Huitle, C. A. & Panizza, M. Electrochemical oxidation of organic pollutants for wastewater treatment. *Curr. Opin. Electrochem.* **11**, 62–71 (2018).

85. Aliyari, M. & Ghanbari, Kh. Highly Sensitive and Selective Electrochemical Determination of Uric Acid in the Presence of Ascorbic Acid and Dopamine Using a Copper Nanoparticle-Tartrazine Nanocomposite Modified Glassy Carbon Electrode by Differential Pulse Voltammetry. *Anal. Lett.* **56**, 1081–1101 (2023).

86. Mcbride, M. & Murray, N. Environmental Factors Governing Corrosion Rates on Overhead Transmission Structures, Hardware and Conductors. (2011).

87. Mirceski, V., Skrzypek, S. & Stojanov, L. Square-wave voltammetry. *ChemTexts* **4**, 17 (2018).

88. Kutchan, T. M. & Dittrich, H. Characterization and Mechanism of the Berberine Bridge Enzyme, a Covalently Flavinylated Oxidase of Benzophenanthridine Alkaloid Biosynthesis in Plants. *J. Biol. Chem.* **270**, 24475–24481 (1995).

89. Zhu, Y.-C. *et al.* Chapter 8 - Enzyme-Based Biosensors and Their Applications. in *Advances in Enzyme Technology* (eds. Singh, R. S., Singhania, R. R., Pandey, A. & Larroche, C.) 201–223 (Elsevier, 2019). doi:10.1016/B978-0-444-64114-4.00008-X.

90. Zhang, J. *et al.* Ratiometric Electrochemical Determination of Ascorbic Acid Using a Copper Nanoparticle@Resin Nanosphere (CuNPs@RNS) Modified Glassy Carbon Electrode (GCE) by Differential Pulse Voltammetry (DPV). *Anal. Lett.* **56**, 2649–2660 (2023).

91. Zablocka, I., Wysocka-Zolopa, M. & Winkler, K. Electrochemical Detection of Dopamine at a Gold Electrode Modified with a Polypyrrole–Mesoporous Silica Molecular Sieves (MCM-48) Film. *Int. J. Mol. Sci.* **20**, 111 (2018).

92. Karakaya, S. & Dilgin, Y. Disposable and Sensitive Electrochemical Determination of Molnupiravir at a Pencil Graphite Electrode (PGE) by Differential Pulse Voltammetry (DPV). *Anal. Lett.* **0**, 1–14 (2023).

93. Nabil, A. *et al.* A Green Voltammetric Determination of Molnupiravir Using a Disposable Screen-Printed Reduced Graphene Oxide Electrode: Application for Pharmaceutical Dosage and Biological Fluid Forms. *Chemosensors* **11**, 471 (2023).

94. Stanković, D. M. *et al.* Point-of-care amperometric determination of L-dopa using an inkjet-printed carbon nanotube electrode modified with dandelion-like MnO2 microspheres. *Microchim. Acta* **186**, 532 (2019).

95. Lindsay, S. *et al.* Discrete microfluidics with electrochemical detection. *Analyst* **132**, 412–416 (2007).

96. Gu, S. *et al.* A droplet-based microfluidic electrochemical sensor using platinum-black microelectrode and its application in high sensitive glucose sensing. *Biosens. Bioelectron.* **55**, 106–112 (2014).

97. Rattanarat, P. *et al.* Graphene-polyaniline modified electrochemical droplet-based microfluidic sensor for high-throughput determination of 4-aminophenol. *Anal. Chim. Acta* **925**, 51–60 (2016).

98. Venton, B. J. & DiScenza, D. J. Chapter 3 - Voltammetry. in *Electrochemistry for Bioanalysis* (ed. Patel, B.) 27–50 (Elsevier, 2020). doi:10.1016/B978-0-12-821203-5.00004-X.

99. Simões, F. R. & Xavier, M. G. 6 - Electrochemical Sensors. in *Nanoscience and its Applications* (eds. Da Róz, A. L., Ferreira, M., de Lima Leite, F. & Oliveira, O. N.) 155–178 (William Andrew Publishing, 2017). doi:10.1016/B978-0-323-49780-0.00006-5.

100. Gurudatt, N. G. *et al.* Electrochemical detection and analysis of tumor-derived extracellular vesicles to evaluate malignancy of pancreatic cystic neoplasm using integrated microfluidic device. *Biosens. Bioelectron.* **226**, 115124 (2023).

101. Kekedy-Nagy, L., Perry, J., Little, S., Ymbern, O. & Shih, S. An electrochemical aptasensor for Δ9-tetrahydrocannabinol detection in saliva on a microfluidic platform. *Biosens. Bioelectron.* **222**, 114998 (2022).

102. Zhou, L. *et al.* In Situ Single-Cell Stimulation and Real-Time Electrochemical Detection of Lactate Response Using a Microfluidic Probe. *Anal. Chem.* **93**, 8680–8686 (2021).

103. Liberti, M. V. & Locasale, J. W. The Warburg Effect: How Does it Benefit Cancer Cells? *Trends Biochem. Sci.* **41**, 211–218 (2016).

104. Zhou, T., Michaels, M. & Kulinsky, L. Guided Healing of Damaged Microelectrodes via Electrokinetic Assembly of Conductive Carbon Nanotube Bridges. *Micromachines* **12**, 405 (2021).

105. Xu, Z. *et al.* A conducting polymer PEDOT:PSS hydrogel based wearable sensor for accurate uric acid detection in human sweat. *Sens. Actuators B Chem.* **348**, 130674 (2021).

106. Navaee, A., Salimi, A. & Teymourian, H. Graphene nanosheets modified glassy carbon electrode for simultaneous detection of heroine, morphine and noscapine. *Biosens. Bioelectron.* **31**, 205–211 (2012).

107. Salimi, A., Hallaj, R. & Khayatian, G.-R. Amperometric Detection of Morphine at Preheated Glassy Carbon Electrode Modified with Multiwall Carbon Nanotubes. *Electroanalysis* **17**, 873–879 (2005).

108. Mashadizadeh, M. H., Abdollahi, G. & Yousefi, T. SmHCF/multiwalled carbon nanotube modified glassy carbon electrode for the determination of codeine. *J. Electroanal. Chem.* **780**, 68–74 (2016).

109. Winkler, A. *et al.* Berberine bridge enzyme catalyzes the six electron oxidation of (S)-reticuline to dehydroscoulerine. *Phytochemistry* **70**, 1092–1097 (2009).

110. Puri, P., Kumar, V., Belgamwar, S. U. & Sharma, N. N. Microfluidic Device for Cell Trapping with Carbon Electrodes Using Dielectrophoresis. *Biomed. Microdevices* **20**, 102 (2018).

111. Gross, E. M., Lowry, E. R., Schaffer, L. V. & Henry, C. S. Electrogenerated Chemiluminescent Detection of Polyamines on a Microfluidic Device Using Micromolded Carbon Paste Microelectrodes. *Electroanalysis* **34**, 1928–1935 (2022).

112. Chen, J. *et al.* Automatic Mode Transition Enabled Robust Triboelectric Nanogenerators. *ACS Nano* **9**, 12334–12343 (2015).

113. Tahir, M. *et al.* Boosting the electrochemical performance and reliability of conducting polymer microelectrode via intermediate graphene for on-chip asymmetric micro-supercapacitor. *J. Energy Chem.* **49**, 224–232 (2020).

114. Ariati, R., Sales, F., Souza, A., Lima, R. A. & Ribeiro, J. Polydimethylsiloxane Composites Characterization and Its Applications: A Review. *Polymers* **13**, 4258 (2021).

115. Yu, H., Balogun, O., Li, B., Murray, T. W. & Zhang, X. Building embedded microchannels using a single layered SU-8, and determining Young's modulus using a laser acoustic technique. *J. Micromechanics Microengineering* **14**, 1576 (2004).

116. Sanchez-Amaya, M. *et al.* Effect of Wide Ranges of Polarization and Concentration on the Behavior of Ferricyanide/Ferrocyanide Systems Studied Through Electrochemical Measurements. *Int. J. Electrochem. Sci.* **17**, 22016 (2022).

117. Cheah, M. H. & Chernev, P. Electrochemical oxidation of ferricyanide. *Sci. Rep.* **11**, 23058 (2021).

118. Niranjana, E., Kumara Swamy, B. E., Raghavendra Naik, R., Sherigara, B. S. & Jayadevappa, H. Electrochemical investigations of potassium ferricyanide and dopamine by sodium dodecyl sulphate modified carbon paste electrode: A cyclic voltammetric study. *J. Electroanal. Chem.* **631**, 1–9 (2009).

119. Dock, E. & Ruzgas, T. Screen-Printed Carbon Electrodes Modified with Cellobiose Dehydrogenase: Amplification Factor for Catechol vs. Reversibility of Ferricyanide. *Electroanalysis* **15**, 492–498 (2003).

120. Krishnaveni, P. & Ganesh, V. Electron transfer studies of a conventional redox probe in human sweat and saliva bio-mimicking conditions. *Sci. Rep.* **11**, 7663 (2021).

121. Morrin, A., Killard, A. J. & Smyth, M. R. Electrochemical Characterization of Commercial and Home-Made Screen-Printed Carbon Electrodes. *Anal. Lett.* **36**, 2021–2039 (2003).

122. Toudeshkchoui, M. G. *et al.* Microfluidic devices with gold thin film channels for chemical and biomedical applications: a review. *Biomed. Microdevices* **21**, 93 (2019).

123. Liu, H. & Crooks, R. M. Highly reproducible chronoamperometric analysis in microdroplets. *Lab. Chip* **13**, 1364–1370 (2013).

124. Ostergaard, S., Olsson, L. & Nielsen, J. Metabolic Engineering of Saccharomyces cerevisiae. *Microbiol. Mol. Biol. Rev.* **64**, 34–50 (2000).

125. Chmayssem, A. *et al.* Characterization of the Impact of Classical Cell-culture Media on the Response of Electrochemical Sensors. *Electroanalysis* **34**, 1201–1211 (2022).

126. Liu, N. *et al.* Electrochemical Aptasensor for Ultralow Fouling Cancer Cell Quantification in Complex Biological Media Based on Designed Branched Peptides. *Anal. Chem.* **91**, 8334–8340 (2019).

127. Delic, M. *et al.* The secretory pathway: exploring yeast diversity. *FEMS Microbiol. Rev.* **37**, 872–914 (2013).

128. Hanssen, B. L., Siraj, S. & Wong, D. K. Y. Recent strategies to minimise fouling in electrochemical detection systems. *Rev. Anal. Chem.* **35**, 1–28 (2016).

129. Gera, N., Hussain, M. & Rao, B. M. Protein selection using yeast surface display. *Methods* **60**, 15–26 (2013).

130. Robbins, E. M., Castagnola, E. & Cui, X. T. Accurate and stable chronic in vivo voltammetry enabled by a replaceable subcutaneous reference electrode. *iScience* **25**, 104845 (2022).

131. Cole, R. H. *et al.* Printed droplet microfluidics for on demand dispensing of picoliter droplets and cells. *Proc. Natl. Acad. Sci.* **114**, 8728–8733 (2017).

132. Shahi, P., Kim, S. C., Haliburton, J. R., Gartner, Z. J. & Abate, A. R. Abseq: Ultrahigh-throughput single cell protein profiling with droplet microfluidic barcoding. *Sci. Rep.* **7**, 44447 (2017).

133. Isozaki, A. *et al.* Sequentially addressable dielectrophoretic array for high-throughput sorting of large-volume biological compartments. *Sci. Adv.* **6**, eaba6712 (2020).

134. Lian, J., Schultz, C., Cao, M., HamediRad, M. & Zhao, H. Multi-functional genome-wide CRISPR system for high throughput genotype–phenotype mapping. *Nat. Commun.* **10**, 5794 (2019).

135. Jumper, J. *et al.* Highly accurate protein structure prediction with AlphaFold. *Nature* **596**, 583–589 (2021).

Appendix 1: calculations

Calculation 1-1: size of (S)-reticuline producing CRAPS library

$e=y^g$

Where

e = number of yeast variants

y = number of enzyme variants used to improve (*S*)-reticuline yield[25]

g = number of genes in (*S*)-reticuline biosynthesis pathway[23]

$1.28*10^{37} = 200{,}000^7$

$e = 1.28*10^{37}$

y = 200,000

g = 7

Calculation 1-2: number of well plates required to screen a CRAPS library of (S)-reticuline producing yeast

$p=e/w$

Where

p = number of well plates

y = number of yeast variants

w = number of wells per plates

p = 911

y = 1,400,000

w = 1536

Calculation 1-3: time to measure a CRAPS library of (S)-reticuline producing yeast using LC/MS

y=e*m/525600

Where

y = number of years

e = number of samples (variants)

m = number of minutes per sample

525600 = number of minutes in a year

$(1.28*10^{37})*15/ 525600 = 3.65*10^{32}$

$y = 3.65*10^{32}$

$e = 1.28*10^{37}$

m = 15

Calculation 1-4: (S)-reticuline fraction of total BIA's produced in well plates*

t= r+s

t = total BIAs

r = (S)-reticuline peak area

n = (S)-norcoclaurine peak area

c = (S)-coclaurine peak area

m = (S)-N-Methylcoclaurine peak area

h = (S)-3’-hydroxy-N-methylcoclaurine peak area

s = n+c+m+h

f = r/t

f=0.51

Calculation 1-5: estimated (S)-reticuline fraction of total BIA’s produced in bioreactor*

* data from[23]

t = r+s

f = r/t

T = total BIAs

R = (S)-reticuline g/L

N = (S)-norcoclaurine g/L

C = (S)-coclaurine g/L = N

M = (S)-N-Methylcoclaurine g/L = N/2

H = (S)-3'-hydroxy-N-methylcoclaurine g/L = N/2

S = N+C+M+H

F = r/t

F = 0.71

Appendix 2: equations

Equation 1-1: The Cottrell Equation

$$i = \frac{nFAC_0\sqrt{D}}{\sqrt{\pi t}}$$

where,

I = current, in units of A

n = number of electrons (to reduce/oxidize one molecule of analyte *j*, for example)

F = Faraday constant, 96485 C/mol

A = area of the electrode in cm^2

C_0 = initial concentration of the reducible analyte in mol/cm^3;

D = diffusion coefficient for species *j* in cm^2/s

t = time in s.

Equation 1-2: The Randles–Ševčík equation (for a non-reversible redox process)

$$I_p = 0.496\sqrt{n' + \beta}FCA\sqrt{nF\upsilon D/RT}$$

Where:

I_p = current maximum in amps

n' = the number of electrons prior to the rate determining step

β = the anodic charge transfer coefficient

F = the Faraday Constant in Coulomb mol^{-1}

C = concentration in mol/cm^3

A = electrode area in cm^2

n = the overall number of electrons transferred

υ = scan rate in V/s

D = diffusion coefficient in cm^2/s

R = the Gas Constant in J K−1 mol−1

T = the temperature in K

Appendix 3: supplementary data

Samples	OD600	(S)-reticuline concentration (μM)
Reticuline producing strain (LN1069)	9.11	929.09478
Base strain (BY4741)	10.1	-11.13723667

Table 1-2 cell density and LC/MS measurement of (S)-reticuline produced by yeast

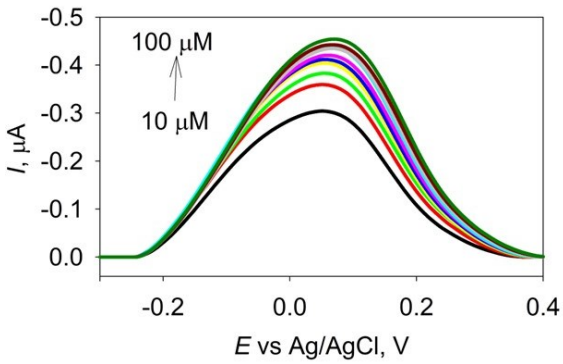

Figure S1 – DPV of (S)-reticuline in YPD media

DPV of (S)-reticuline shows a concentration dependent increases in peak height from 10-100 μM at a glassy carbon working electrode